

Towards accurate nuclear mass tables in covariant density functional theory

A. Taninah,^{1,2} B. Osei,¹ A. V. Afanasjev,¹ U. C. Perera,¹ and S. Teeti¹

¹*Department of Physics and Astronomy, Mississippi State University, MS 39762*

²*Department of Chemistry and Physics, Louisiana State University, Shreveport, LA 71115.*

(Dated: June 5, 2024)

The current investigation focuses on detailed analysis of the anchor based optimization approach (ABOA), its comparison with alternative global fitting protocols and on the global analysis of the truncation of basis effects in the calculation of binding energies. It is shown that ABOA provides a solution which is close to that obtained in alternative approaches but at small portion of their computational time. The application of softer correction function after few initial iterations of ABOA stabilizes and speeds up its convergence. For the first time, the numerical errors in the calculation of binding energies related to the truncation of bosonic and fermionic bases have been globally investigated with respect of asymptotic values corresponding to the infinite basis in the framework of covariant density functional theory (CDFT). These errors typically grow up with the increase of the mass and deformation of the nuclei. To reduce such errors in bosonic sector below 10 keV for almost all nuclei with proton number $Z < 120$ one should truncate the bosonic basis at $N_B = 28$ instead of presently used $N_B = 20$. The reduction of the errors in binding energies due to the truncation of the fermionic basis in CDFT is significantly more numerically costly. For the first time it is shown that the pattern and the speed of the convergence of binding energies as a function of the size of fermionic basis given by N_F depend on the type of covariant energy density functional. The use of explicit density dependence of the meson-nucleon coupling constants or point couplings slows down substantially the speed of convergence of binding energies as a function of N_F . The present paper clearly indicates the need for accounting of infinite basis corrections for accurate calculation of binding energies and for fitting more precise next generation covariant energy density functionals: note that such corrections are neglected in the present generation of the functionals. A new procedure for finding the asymptotic values of binding energies is suggested in the present paper: it allows better control of numerical errors.

I. INTRODUCTION

Nuclear binding energies (or masses) is one of the most fundamental properties of atomic nuclei. In experiment they are studied with extreme relative mass precision of $\delta m/m = 10^{-9}$ and in some nuclei even with precision of 10^{-10} [1, 2]. In absolute terms this corresponds to the accuracy of the measurements of the binding energies better than 1 keV. Accurate knowledge of binding energies is important for nuclear structure, neutrino physics and nuclear astrophysics. The measurements of nuclear masses far from stability provide a fundamental test for our understanding of nuclear structure [1] and the constraints on model predictions for the boundaries of nuclear landscape (see Ref. [3–5]). The measurements of mass differences (Q values) of specific isotopes play a key role in neutrino physics: in order to determine the neutrino mass on a sub-eV level one should measure the Q values of certain β transitions better than 1 eV [2]. Different nuclear astrophysical processes [such as r-process (see Refs. [6, 7]) or the processes in the crust of neutron stars (see Refs. [8, 9])] also sensitively depend on nuclear masses since they affect nuclear reaction rates.

There was a substantial and continuous effort in non-relativistic models to improve the functionals and global reproduction of experimental masses (see, for example, Refs. [10–17] and references quoted therein). Existing global fits of the model parameters to the ground state masses reach an accuracy of ≈ 0.5 MeV in the

global reproduction of experimental masses in the microscopic+macroscopic (mic+mac) approach [14] and in Skyrme density functional theory (DFT) [12] and around 0.8 MeV in the Gogny DFT [18]. These fits take into account the correlations beyond mean field by either adding rotational and vibrational corrections in a phenomenological way or by employing five-dimensional collective Hamiltonian (5DCH). Note that the global fits at the mean field level in the Skyrme DFT lead to 1.4 – 1.9 MeV accuracy in the global description of experimental binding energies (see Refs. [15–17]).

In contrast, the attempts to create covariant energy density functionals (CEDF) based on the global set of data on binding energies are very limited in covariant density functional theory (CDFT). It is only in Refs. [19, 20] that they were undertaken (see Sec. II for more detail). This is due to the fact that the calculations within the CDFT are significantly more numerically challenging and more time-consuming as compared with those carried out in nonrelativistic DFT due to relativistic nature of the CDFT. First, the wavefunctions of the single-particle states in the CDFT are represented by Dirac spinors the large and small components of which have opposite parities. As a consequence, the basis for a given maximum value of principal quantum number N in the basis set expansion has approximately double size in the CDFT as compared with non-relativistic models. As a result, the numerical calculations of matrix elements and the diagonalization of the matrices requires substantially more time than in the case of nonrelativistic DFTs.

A rough estimate provided in Ref. [21] for spherical symmetry indicates that the calculations in the Skyrme DFT and CDFT for a given maximum value of principal quantum number N in the basis set expansion differ by approximately an order of magnitude. Second, the most widely used classes of CEDFs contain the mesons in addition to fermions [5, 22]. This requires the solution of Klein-Gordon equations which adds numerical cost to the calculations. Third, in the CDFT the nucleonic potential (≈ -50 MeV/nucleon) emerges as the sum of very large attractive scalar S (≈ -400 MeV/nucleon) and repulsive vector V ($V \approx 350$ MeV/nucleon) potentials (see Ref. [22]). In the nucleus with mass A , these values are multiplied by A and this leads to a cancellation of very large quantities. This may lead to a slower convergence of binding energies as a function of the size of the basis in the CDFT as compared with non-relativistic DFTs.

Many of the fits of the relativistic and non-relativistic functionals (including global ones) have been carried out using computer codes employing basis set expansion approach in which the wave functions are expanded into the basis of harmonic oscillator wave functions. This expansion is precise for the infinite size of the basis. However, due to numerical reasons the basis is truncated in the calculations. Unfortunately, a rigorous analysis of numerical errors in calculated binding energies emerging from the truncation of basis is missing in global calculations. However, there are some indications that they are not negligible. For example, the relativistic Hartree-Bogoliubov (RHB) calculations of the ground state in ^{208}Pb with DD-ME2 functional indicate that binding energies calculated with $N_F = 20$ fermionic shells deviate from asymptotic value of binding energy B_∞ by approximately 250 keV (see discussion of Fig. 2 in Supplemental Material to Ref. [20]). Note that this difference represents only 0.015% error in the description of total binding energy. In a similar way, total binding energies of the ^{120}Sn and $^{102,110}\text{Zr}$ nuclei obtained in the Skyrme DFT calculations with the SLy4 force in the basis of $N = 20$ and $N = 25$ harmonic oscillator (HO) shells differ by 110-150 keV [24, 25]. Ref. [25] also indicates that the HO basis with $N = 25$ is needed in order to describe the binding energies of the nuclei in this mass region with an accuracy of the couple of tens keV.

Thus, the present paper aims at the investigation of several issues related to the calculations of binding energies with high precision in the CDFT framework. One of the goals is to understand the numerical errors in the calculations of binding energies. In particular, their global dependence on the truncation of the basis both in the fermionic and bosonic sectors of the CDFT will be investigated for the first time. We will also study how these numerical errors depend on the type of the symmetry (spherical versus axially deformed) of the nuclear shape and how the convergence of binding energies as a function of the size of the basis depends on the type of functional. The second goal is to understand to which extent the procedures for the definition of asymptotic binding

energies employed earlier in non-relativistic functionals are applicable in the CDFT. The third goal is to further understand the role and the features of the anchor based optimization method suggested in Ref. [20] as an alternative to other methods of global fitting of the functionals.

The paper is organized as follows. A short review of the approaches to global fitting of the energy density functionals (EDF) is presented in Sec. II. Sec. III provides a brief outline of theoretical formalism and the discussion of major classes of CEDFs under study. A discussion of the anchor based approach to the optimization of energy density functionals and its comparison with alternative methods for global fitting of the functionals is given in Sec. IV. The impact of the truncation of basis in bosonic and fermionic sectors of the CDFT on binding energies as well as asymptotic behavior of the calculated binding energies are analysed in Sec. V. A new method of defining asymptotic values of calculated binding energies is presented in Sec. VI. Finally, Sec. VII summarizes the results of our paper.

II. A REVIEW OF APPROACHES TO GLOBAL FITTING OF FUNCTIONALS

The analysis of literature reveals that at present there are three different approaches to global fitting of energy density functionals. These are

- **Fully Global Approach (further FGA).** In the FGA the optimization of the functional is performed using computer codes which include either axial or triaxial deformation. It allows to use in fitting protocol the quantities which depend on deformation such as fission barriers which are not accessible in alternative fitting protocols.
- **Reduced Global Approach (further RGA)** has been outlined in Sec. II of Ref. [10]. The specific feature of this approach is the fact that the deformation effects are taken into account in deformed and transitional nuclei by calculating the deformation energy E_{def}

$$E_{def}(Z, N) = E_{sph}(Z, N) - E_{eq}(Z, N) \quad (1)$$

where E_{eq} is the energy at the equilibrium deformation and E_{sph} is the energy of spherical configuration. The E_{def} values are calculated using axially deformed code and then all experimental binding energies are renormalized to their "equivalent spherical configuration" values. Then, the rms errors of the current iteration of the functional are calculated using a spherical code by comparing the binding energies it gives with these *renormalized* experimental binding energies. Thus, each iteration of optimization consists of defining the E_{def} in deformed code and fitting the functional in spherical code. However, to reach an optimal fit one

should repeat iterations until full convergence of $E_{def}(Z, N)$ is reached.

- **Anchor Based Optimization Approach (further ABOA).** In the ABOA (see Ref. [20]), the optimization of the parameters of EDFs is carried out for a selected set of spherical anchor nuclei, the physical observables of which are modified by the correction function

$$E_{corr}(Z, N) = \alpha_i(N - Z) + \beta_i(N + Z) + \gamma_i \quad (2)$$

which takes into account the global performance of EDFs. Here i is the counter of the iteration in the anchor-based optimization. The parameters α_i and β_i correct the deficiencies of EDF in isospin and in mass number while γ_i is responsible for a global shift in binding energies¹.

Each of these approaches has its own advantages and disadvantages which are discussed below.

The FGA potentially allows to avoid all uncertainties related to the selection of nuclei used in the fitting protocol and allows to use the physical quantities which depend on deformation (such as the height of fission barriers) in fitting protocol. However, the calculations in deformed codes are extremely numerically expensive and computational time does not depend drastically on the selection of the functional (see Table I). For example, within the CDFT framework the numerical calculations in deformed RHB code are by more than two orders of magnitude more time consuming than those in spherical RHB one for the fermionic basis characterized by full $N_F = 16$ fermionic shell (see columns 4 and 5 in Table II). Further increase of fermionic basis leads to a drastic increase of the ratio of the calculational time in deformed and spherical RHB calculations: this ratio is approaching three orders of magnitude at $N_F = 18$ (see Table II). The simplification of the code by the transition to the relativistic mean field (RMF)+BCS framework does not change much this ratio. Similar situation holds also in non-relativistic Skyrme and Gogny DFT.

The FGA has been used in the number of studies but there are two possible ways of its application. In the first method, a large basis is used to reduce numerical errors in the calculations of binding energies but this restricts the number of the nuclei which can be included in the fitting protocol. However, the lack of strict mathematical procedure in the selection of nuclei leads to some subjectivity and possibly to some biased errors. This problem can be reduced by the inclusion of a larger set of nuclei into the fitting protocol. However, the computational cost raises drastically so that the increase of the

TABLE I. Average computational time per nucleus (in CPU-hours) in axially deformed RHB code as a function of the size of fermionic basis (given by N_F) for indicated CEDFs. It is defined for the ground states of the set of 100 nuclei more or less equally distributed over the part of nuclear chart for which experimental data are available. Note that as a rule computational time increases for the deformations of the basis deviating from the equilibrium one.

N_F	Computational time per nucleus [CPU-hours]			
	DD-MEX	DD-PC1	NL5(E)	PCPK1
16	0.26	0.15	0.19	0.19
18	0.51	0.35	0.40	0.39
20	1.05	0.68	0.68	0.68
22	2.02	0.98	1.43	1.22
24	3.36	2.02	2.57	2.66
26	5.17	4.08	4.48	4.20
28	8.21	6.39	7.77	7.49
30	15.94	11.11	13.34	11.66

TABLE II. Columns (2) and (3): the same as in Table I but for the calculations in spherical RHB code for the same set of 100 nuclei. Columns (4) and (5) show the ratio of computational time in deformed and spherical RHB calculations.

N_F	Computational time per nucleus [CPU-hours]		Ratio	
	2	3	4	5
	DD-MEX	DD-PC1	DD-MEX	DD-PC1
16	0.000440	0.000238	590.91	630.25
18	0.000596	0.000365	855.70	958.90
20	0.000646	0.000590	1625.39	1152.54
22	0.001233	0.000700	1638.28	1400.00
24	0.001654	0.000953	2031.44	2119.62
26	0.002163	0.001264	2390.20	3227.85
28	0.002401	0.001634	3419.41	3910.65
30	0.002758	0.001983	5779.55	5602.62

number of nuclei leads to a substantial reduction of the basis size used in the calculations because of the limitations imposed on availability of computational resources. This, in turn requires the use of approximate relations to find the asymptotic value of the binding energy corresponding to infinite size of basis (see Sec. V for details). Thus, a very large number of the nuclei is used in the fitting protocol of the second method but this requires the use of moderate basis in numerical calculations and approximate relations to find the asymptotic value of the binding energy corresponding to infinite size of basis.

For example, the first method was used in Refs. [15–17] in Skyrme DFT for the development of the UNEDF class of the functionals. Note that fitting protocol of the UNEDF1 and UNEDF2 functionals has been supplemented by information on fission barriers and single-particle energies, respectively. In all optimizations, the large spherical basis with 20 harmonic oscillator shells ($N = 20$) was used which led to quite substantial computational time in the calculations with deformed HFBTHO code. As a consequence, a limited number of nuclei (approximately 28 spherical and 46 deformed) were used in these

¹ Note that similar in spirit approach is used in Ref. [26] in which the quadrupole zero-point energy is replaced by a constant binding energy shift [similar to the γ_i term in Eq. (2)] which is fixed by minimizing the global rms deviation.

optimizations.

The second method has been used in the fitting protocol of the BCPM (Barcelona-Catania-Paris-Madrid) functional (see Ref. [13]). It included 579 measured masses of even-even nuclei and the calculations have been carried out in a reduced basis which takes into account eleven harmonic oscillator shells for the $Z < 50$ nuclei, 13 shells for the $50 < Z < 82$ nuclei, and 15 shells for $Z > 82$ nuclei. Another example is the D1M and D1M* functionals which were fitted to 2149 and 620 nuclei, respectively, in axially deformed calculations corrected by quadrupole corrections to total binding energy and infinite-basis corrections ΔB_∞ [see Eq. (27) below] in Refs. [18, 26]. Note that only even-even nuclei were considered in the fit of the D1M* functional. The axially deformed calculations for these two functionals were performed in the basis with $N \leq 14$ major oscillator shells.

There is also a hybrid method which was used in the fitting of the DD-MEB1 and DD-MEB2 CEDFs in Refs. [19]: this fitting protocol contains 2353 experimental masses. The minimization of these functionals was performed in axially deformed RHB code with $N_F = 16$ fermionic shells but with calculated binding energies corrected before and after minimization by the difference between the results obtained with $N_F = 16$ and $N_F = 20$ (see Ref. [27]).

The RGA has been used in the fitting protocol of the BSk1-32 series of the Skyrme functionals using very large bases (see, for example, Refs. [11, 12, 28, 29]). For instance, it consisted of the $N = 25$ HO shells in spherical calculations and $N = 21$ HO shells in deformed calculations in Ref. [11]. This allows to keep numerical error in calculated masses relatively low without involving the correction for infinite basis size. Note that fitting protocols of these functionals typically include all nuclei for which experimental data on binding energies is available.

The ABOA has been introduced in Ref. [20]. It was shown that the use of this approach leads to a substantial improvement in the global description of binding energies for several classes of CEDFs (see also Sec. IV A below). This approach leads to the results which are comparable to those obtained in RGA (see Ref. [20] and the discussion in Sec. IV C). The computational cost of defining a new functional within this approach is drastically lower as compared with FGA and RGA and this aspect is discussed in detail in Sec. IV B below. It turns out that the use of twelve anchor spherical nuclei distributed over the nuclear chart in the optimization is sufficient for this approach (see Ref. [20]). Note that existing optimizations of CEDFs within the ABOA have been obtained in the RHB calculations with $N_F = 20$ fermionic and $N_B = 20$ bosonic shells (see Ref. [20]). Such a truncation of the basis is used also in other recent CEDF optimizations²

(see, for example, Refs. [30, 31]). However, there are also the cases when smaller basis was used: for example, the DD-PC1 functional has been defined in deformed calculations with $N_F = 16$ fermionic shells [32].

It is necessary to mention that in these investigations the numerical errors in the binding energies associated with the truncation of basis or the definition of their asymptotic values have been either discussed only for a few selected nuclei or not mentioned at all. Thus, at present there is no published information on how these errors evolve across the nuclear landscape and how they depend on the type of the functional or theory employed. Thus, one of the goals of the present study is to close this gap in our knowledge in the CDFT framework.

III. THEORETICAL FRAMEWORK

The calculations were performed in the framework of relativistic Hartree-Bogoliubov (RHB) approach the technical details on the solution of which can be found in Refs. [5, 22, 33]. The calculations were carried out with two versions of the RHB code suitable for spherical and axially deformed nuclei, respectively. Both codes allow the calculations with a wide range of covariant energy density functionals. We employ a parallel version of the axial RHB computer code developed in Ref. [5]: it allows simultaneous calculations for a significant number of nuclei and deformation points in each nucleus. The unconstrained calculations are performed in axial RHB code using four initial deformations of the basis $\beta_2 = -0.2, 0.0, 0.2$ and 0.4 . As follows from the comparison with the calculations constrained on β_2 this procedure guarantees finding the lowest in energy minimum but it is substantially less numerically costly as compared with constrained calculations.

Both spherical and axial RHB computer codes are based on the expansion of the Dirac spinors and the meson fields in terms of harmonic oscillator wave functions with respective symmetry [so-called basis set expansion method] (see Ref. [33, 34]). We illustrate here this expansion for the case of axially deformed nuclei (see Refs. [33, 34] for more details and for the case of spherical symmetry).

The single-particle wave function $\psi_i(\vec{r}, s, t)$ of the nucleon in the state i , which follows from the solution of the Dirac equation, is given by

$$\psi_i(\vec{r}, s, t) = \begin{pmatrix} f_i(\vec{r}, s, t) \\ ig_i(\vec{r}, s, t) \end{pmatrix} \quad (3)$$

where the large ($f_i(\vec{r}, s, t)$) and small ($g_i(\vec{r}, s, t)$) components of a Dirac spinor are expanded independently in

² Unfortunately, the majority of the papers dedicated to the optimization of CEDFs do not explicitly provide information on the size of the basis used in the fitting protocols.

terms of the HO eigenfunctions $\Phi_\alpha(\vec{r}, s)$

$$f_i(\vec{r}, s, t) = \sum_{\alpha}^{\alpha_{max}} f_{\alpha}^{(i)} \Phi_{\alpha}(\vec{r}, s) \chi_{t_i}(t) \quad (4)$$

$$g_i(\vec{r}, s, t) = \sum_{\tilde{\alpha}}^{\tilde{\alpha}_{max}} f_{\tilde{\alpha}}^{(i)} \Phi_{\tilde{\alpha}}(\vec{r}, s) \chi_{t_i}(t). \quad (5)$$

The HO eigenfunctions have the form (see Ref. [33])

$$\Phi_{\alpha}(\vec{r}, s) = \varphi_{n_z}(z, b_z) \varphi_{n_r}^{\Lambda}(r_{\perp}, b_{\perp}) \frac{e^{i\Lambda\phi}}{\sqrt{2\pi}} \chi(s) \quad (6)$$

where n_z and n_r are the number of nodes in the z - and r_{\perp} - directions, respectively, and Λ and m_s are projections of the orbital angular momentum and spin on the intrinsic z -axis, respectively. b_z and b_{\perp} are oscillator lengths in respective directions.

The quantum numbers $|\alpha\rangle = |n_z n_r \Lambda s\rangle$ and $|\tilde{\alpha}\rangle = |\tilde{n}_z \tilde{n}_r \tilde{\Lambda} \tilde{s}\rangle$ in the sums of Eqs. (4) and (5) run over all permitted combinations of n_z and n_r , Λ and m_s (and their tilted counterparts) defined by the truncation of the basis. In absolute majority of the CDFT calculations, full fermionic HO shells are used in the basis set expansion and we follow this prescription in the present paper. Thus, α_{max} is selected in such a way that all basis states corresponding to full $N_F = 2n_r + |\Lambda| + n_z$ fermionic shells are included into the basis of large components. The basis of small components includes $N_F + 1$ full fermionic shells to avoid spurious contributions to the RHB equation (see Ref. [34] for details). Note that large and small components of the Dirac spinor have opposite parities: this leads to an approximate doubling of the basis in the CDFT as compared with non-relativistic theories.

The solution of the Klein-Gordon equation is obtained by expanding mesonic fields in a complete set of basis states [HO eigenfunctions] along $[\varphi_{n_z}(z, b_z)]$ and perpendicular $[\varphi_{n_r}^0(r_{\perp}, b_{\perp})]$ the axis of symmetry of the nucleus

$$\phi(z, r_{\perp}) = \sum_{n_z n_r}^{N_B} \phi_{n_z n_r} \varphi_{n_z}(z, b_z) \varphi_{n_r}^0(r_{\perp}, b_{\perp}) \quad (7)$$

This expansion is truncated at full N_B bosonic shells.

The spherical RHB code is not parallelized but it allows the calculations to a very large value of $N_F = 38$ (see Sec. VB below). Thus, the convergence of the results of the calculations in spherical nuclei as a function of N_F has been tested using this code. In contrast, the axial RHB code works only up to $N_F = 30$ due to memory allocation problems at larger values of N_F . Note that similar to Fig. 2 of Supplemental Material to Ref. [20] we verified for selected set of spherical and deformed nuclei that the codes developed in our group and those existing in the DIRHB package of the RHB codes (see Ref. [33]) provide almost the same (within a few keVs) results for binding energies as a function of N_F and N_B . Note that only DD-ME* and DD-PC* types of the functionals are included into the DIRHB codes of Ref. [33].

In order to understand the dependence of the convergence properties on the functional we consider three major classes of CEDFs used at present. These are (i) those based on meson exchange with non-linear meson couplings (NLME) (see Ref. [35]), (ii) those based on meson exchange with density dependent meson-nucleon couplings (DDME) (see Ref. [36]), and finally (iii) those based on point coupling (PC) models containing various zero-range interactions in the Lagrangian (see Ref. [37]).

The Lagrangians of these three major classes of CEDFs can be written as: $\mathcal{L} = \mathcal{L}_{common} + \mathcal{L}_{model-specific}$ where the \mathcal{L}_{common} consist of the Lagrangian of the free nucleons and the electromagnetic interaction. It is identical for all three classes of functionals and is written as

$$\mathcal{L}_{common} = \mathcal{L}^{free} + \mathcal{L}^{em} \quad (8)$$

with

$$\mathcal{L}^{free} = \bar{\psi}(i\gamma_{\mu}\partial^{\mu} - m)\psi \quad (9)$$

and

$$\mathcal{L}^{em} = -\frac{1}{4}F^{\mu\nu}F_{\mu\nu} - e\frac{1-\tau_3}{2}\bar{\psi}\gamma^{\mu}\psi A_{\mu}. \quad (10)$$

For each model there is a specific term in the Lagrangian: for the DDME models we have

$$\begin{aligned} \mathcal{L}_{DDME} = & \frac{1}{2}(\partial\sigma)^2 - \frac{1}{2}m_{\sigma}^2\sigma^2 - \frac{1}{4}\Omega_{\mu\nu}\Omega^{\mu\nu} + \frac{1}{2}m_{\omega}^2\omega^2 \\ & - \frac{1}{4}\vec{R}_{\mu\nu}\vec{R}^{\mu\nu} + \frac{1}{2}m_{\rho}^2\vec{\rho}^2 - g_{\sigma}(\bar{\psi}\psi)\sigma \\ & - g_{\omega}(\bar{\psi}\gamma_{\mu}\psi)\omega^{\mu} - g_{\rho}(\bar{\psi}\vec{\tau}\gamma_{\mu}\psi)\vec{\rho}^{\mu} \end{aligned} \quad (11)$$

with the density dependence of the coupling constants given by

$$g_i(\rho) = g_i(\rho_0)f_i(x) \quad \text{for } i = \sigma, \omega \quad (12)$$

$$g_{\rho}(\rho) = g_{\rho}(\rho_0)\exp[-a_{\rho}(x-1)] \quad (13)$$

where ρ_0 denotes the saturation density of symmetric nuclear matter and $x = \rho/\rho_0$. The functions $f_i(x)$ are given by the Typel-Wolter ansatz [36]

$$f_i(x) = a_i \frac{1 + b_i(x + d_i)}{1 + c_i(x + d_i)}. \quad (14)$$

Because of the five conditions $f_i(1) = 1$, $f_i''(1) = 0$, and $f_{\sigma}''(1) = f_{\omega}''(1)$, only three of the eight parameters a_i , b_i , c_i , and d_i are independent and we finally have the four parameters b_{σ} , c_{σ} , c_{ω} , and a_{ρ} characterizing the density dependence. In addition we have the four parameters of the Lagrangian \mathcal{L}_{DDME} m_{σ} , g_{σ} , g_{ω} , and g_{ρ} . As usual the masses of the ω - and the ρ -meson are kept fixed at the values $m_{\omega} = 783$ MeV and $m_{\rho} = 763$ MeV [38, 39]. We therefore have $N_{par} = 8$ parameters in the DDME class of the models. The DD-MEX [31], DD-ME2 [38] and DD-MEY [20] functionals have been used in the present study.

The NLME class of the functionals has the same model specific Lagrangian as the DDME class except that the coupling constants g_σ , g_ω , and g_ρ are constants and there are extra terms for a non-linear σ meson coupling. These couplings are important for the description of surface properties of finite nuclei, especially the incompressibility [35] and for nuclear deformations [34].

$$\mathcal{L}_{NLME} = \mathcal{L}_{DDME} - \frac{1}{3}g_2\sigma^3 - \frac{1}{4}g_3\sigma^4 \quad (15)$$

For the NLME class we have $N_{par} = 6$ parameters m_σ , g_σ , g_ω , g_ρ , g_2 , and g_3 . In the present study, we use the NL5(E) CEDF from Ref. [40].

In general, the Lagrangian of the PC models contains three parts:

(i) the four-fermion point coupling terms:

$$\begin{aligned} \mathcal{L}^{4f} = & -\frac{1}{2}\alpha_S(\bar{\psi}\psi)(\bar{\psi}\psi) - \frac{1}{2}\alpha_V(\bar{\psi}\gamma_\mu\psi)(\bar{\psi}\gamma^\mu\psi) \\ & - \frac{1}{2}\alpha_{TS}(\bar{\psi}\vec{\tau}\psi)(\bar{\psi}\vec{\tau}\psi) - \frac{1}{2}\alpha_{TV}(\bar{\psi}\vec{\tau}\gamma_\mu\psi)(\bar{\psi}\vec{\tau}\gamma^\mu\psi), \end{aligned} \quad (16)$$

(ii) the gradient terms which are important to simulate the effects of finite range:

$$\begin{aligned} \mathcal{L}^{der} = & -\frac{1}{2}\delta_S\partial_\nu(\bar{\psi}\psi)\partial^\nu(\bar{\psi}\psi) \\ & - \frac{1}{2}\delta_V\partial_\nu(\bar{\psi}\gamma_\mu\psi)\partial^\nu(\bar{\psi}\gamma^\mu\psi) \\ & - \frac{1}{2}\delta_{TS}\partial_\nu(\bar{\psi}\vec{\tau}\psi)\partial^\nu(\bar{\psi}\vec{\tau}\psi) \\ & - \frac{1}{2}\delta_{TV}\partial_\nu(\bar{\psi}\vec{\tau}\gamma_\mu\psi)\partial^\nu(\bar{\psi}\vec{\tau}\gamma^\mu\psi), \end{aligned} \quad (17)$$

(iii) The higher order terms which are responsible for the effects of medium dependence

$$\begin{aligned} \mathcal{L}^{hot} = & -\frac{1}{3}\beta_S(\bar{\psi}\psi)^3 - \frac{1}{4}\gamma_S(\bar{\psi}\psi)^4 \\ & - \frac{1}{4}\gamma_V[(\bar{\psi}\gamma_\mu\psi)(\bar{\psi}\gamma^\mu\psi)]^2. \end{aligned} \quad (18)$$

However, the structure of two PC functionals, namely, PC-PK1 and DD-PC1, employed in the present paper depends on particular realization of this scheme. The PC-PK1 CEDF closely follows this scheme but it neglects the scalar-isovector channel, i.e. $\alpha_{TS} = \delta_{TS} = 0$. This is because the information on masses and charge radii of finite nuclei does not allow one to distinguish the effects of the two isovector mesons δ and ρ (see Ref. [39]). Thus, for this PC CEDF we have $N_{par} = 9$ parameters α_S , α_V , α_{TV} , δ_S , δ_V , δ_{TV} , β_S , γ_S , γ_V . The DD-PC1 functional [32] introduces the density dependence of the α_S , α_V and α_{TV} constants via

$$\alpha_i(\rho) = a_i + (b_i + c_i x)e^{-d_i x} \quad (\text{for } i = S, V, TV), \quad (19)$$

and eliminates the terms proportional to α_{TS} , δ_{TS} [this is similar to the PC-PK1 functional] and δ_V , δ_{TV} , β_S , γ_S

and γ_V in Eqs. (16-18). The introduced density dependence of the α_S , α_V and α_{TV} constants partially takes care of the impact of omitted terms. Note that in the isovector channel a pure exponential dependence is used, i.e. $a_{TV} = c_{TV} = 0$. Thus, the DD-PC1 functional contains the $N_{par} = 10$ parameters, i.e. a_S , b_S , c_S , d_S , a_V , b_V , c_V , d_V , b_{TV} and d_{TV} .

Note that in the deformed RHB calculations we use $ngh = 30$ and $ngl = 30$ integration points in the Gauss-Hermite and Gauss-Laguerre quadratures in the $z > 0$ and $r_\perp > 0$ directions, respectively, in order to properly take into account the details of the single-particle wave functions. The same $ngh = 30$ is used in the Gauss-Hermite quadratures for $r > 0$ in spherical RHB calculations.

The experimental binding energies of twelve anchor spherical nuclei (^{16}O , $^{40,48}\text{Ca}$, ^{72}Ni , ^{90}Zr , $^{116,124,132}\text{Sn}$, $^{204,208,214}\text{Pb}$ and ^{210}Po) and charge radii of nine of them (namely, ^{16}O , $^{40,48}\text{Ca}$, ^{90}Zr , $^{116,124}\text{Sn}$ and $^{204,208,214}\text{Pb}$) are used in the anchor based optimization approach (see Ref. [20] for more details). The correction function of Eq. (2) is defined in ABOA using 855 even-even nuclei for which experimental binding energies are available in Ref. [41].

IV. FURTHER DISCUSSION OF ANCHOR-BASED OPTIMIZATION APPROACH

The anchor-based optimization of energy density functionals is defined in Ref. [20] and the basic results for this approach have been discussed in this reference and in Supplemental Material to it. It is based on the introduction of the correction function $E_{corr}(Z, N)$ given in Eq. (2) by which the binding energies of spherical anchor nuclei are redefined for global performance of the EDFs (see Ref. [20]) for full details). The behavior of these parameters during the iterative procedure has been illustrated for the DD-MEX1, DD-MEY and NL5(Y) functionals in Tables I, II and III of the Supplemental Material to Ref. [20]. In addition, the evolution of the rms deviations ΔE_{rms} between calculated and experimental binding energies E for these functionals during the iterative procedure was also illustrated in Fig. 1 of Supplemental Material to Ref. [20].

In this section we extend the discussion of the ABOA to other functionals, introduce new improved strategy for the fitting of the functionals within ABOA, provide an estimate of the computation time for the ABOA and RGA approaches and compare the results obtained for the DD-MEY type of the functionals in the RGA and ABOA.

A. Further improvement of the convergence of the ABOA

Figure 1 of Supplemental Material to Ref. [20] [see also black curve in Fig. 1(c)] shows a significant increase in global ΔE_{rms} at the 4th iteration of the convergence process. This indicates that the push provided by the correction function of Eq. (2) is too strong. It turns out that this problem can be eliminated by switching to a softer correction function

$$E_{corr}^{mod}(Z, N) = \frac{\alpha_i}{2}(N - Z) + \frac{\beta_i}{2}(N + Z) + \frac{\gamma_i}{2} \quad (20)$$

after few initial iterations in the convergence process. Note that the convergence of the iterative procedure is reached in the limit $\alpha_i \rightarrow 0$, $\beta_i \rightarrow 0$, and $\gamma_i \rightarrow 0$.

The advantage of this modified procedure is illustrated in Fig. 1(c) on the example of the DD-MEX1 functional. The use of correction function $E_{corr}(Z, N)$ leads to the convergence curve for ΔE_{rms} shown in black color which is characterized by a large peak at the 4th iteration and which requires 14 iterations for a convergence. However, the switch to $E_{corr}^{mod}(Z, N)$ at the 3^d iteration eliminates this peak and reduces the number of required iterations to seven (see red curve in Fig. 1(c) and Table III). Thus, the combination of these two correction functions leads to a rapid and smooth convergence process: the $E_{corr}(Z, N)$ function provides a significant push so that only one to three iterations are needed to drive the functional towards its minimum in the parameter hyperspace in the beginning of iterative process and $E_{corr}^{mod}(Z, N)$ guaranties the smoothness of convergence process at further iterations.

This combined procedure has also been used in the fit of the PC-Y and PC-Y1 functionals defined in Ref. [20]. Figs. 1(a) and (b) and Tables IV and V illustrate that drastic improvement of the global performance of these functionals was reached after first iteration and then additional few iterations provide only minor improvement of the functionals.

B. The dependence of computational time on approach

It is interesting to compare the computer resources required for definition of the functional in different approaches. The numbers quoted below are based on the RHB calculations with $N_F = 20$ and $N_B = 20$. Numerical calculations are performed at Orion of High Performance Computing Collaboratory (HPC²) of Mississippi State University (see <https://www.hpc.msstate.edu/computing/hpc.php>) and they reflect the computation time allocation of this facility. The largest standard allocation per user is 400 CPU with 48 hours execution time limit; it is utilized in most of our calculations.

TABLE III. The values of the parameters α_i , β_i and γ_i of Eqs. (2) and (20) defined at the i -th iteration during the iterative procedure of the anchor based optimization method. The results are presented for iterative procedure of the DD-MEX1 functional. ΔE_{rms} is global rms deviation of binding energies at i -th iteration. The steps of iterative procedure for which the correction functions of Eqs. (2) and (20) are used are shown in bold and plain text, respectively.

iteration	ΔE_{rms}	α_i	β_i	γ_i
i	[MeV]			
0	2.849	-0.075	0.0235	-3.29
1	2.144	0.044	-0.028	2.55
2	2.139	-0.044	0.026	-2.12
3	1.799	0.045	-0.020	1.70
4	1.653	0.005	0.000	0.05
5	1.654	0.005	0.000	0.05
6	1.675	-0.010	0.000	0.00
7	1.651	0.000	0.000	0.00

TABLE IV. The same as Table I but for the PC-Y functional.

iteration	ΔE_{rms}	α_i	β_i	γ_i
i	[MeV]			
0	3.097	+0.086	-0.036	1.00
1	1.974	-0.003	+0.002	-0.25
2	1.951	-0.002	+0.001	-0.15
3	1.959	0.000	0.000	-0.19
4	2.002	-0.007	0.001	-0.13
5	1.950	0.009	0.004	-0.14
6	1.951	-0.0099	0.004	0.02

Let us start with anchor based optimization approach. The first step in each iteration of ABOA is the optimization of the parameters for 12 anchor spherical nuclei. This is carried out within the simplex method³ starting

TABLE V. The same as Table I but for the PC-Y1 functional.

iteration	ΔE_{rms}	α_i	β_i	γ_i
i	[MeV]			
0	2.698	+0.065	-0.030	1.10
1	1.943	-0.010	0.000	0.20
2	1.953	-0.010	-0.001	0.15
3	1.923	+0.024	-0.001	-0.03
4	1.858	+0.017	-0.002	0.01
5	1.849	+0.001	-0.0001	-0.001

³ The simplex method of the minimization is one of the simplest and fastest ones (see Ref. [42]). The minimizations by the simplex method are prone to end in local minima and that is a reason why, in general, it is not recommended for the search of the global minimum. However, it is our experience that by starting from a reasonable number of randomly generated initial points in parameter hyperspace we always find a global minimum as defined by alternative approaches such as simulated annealing

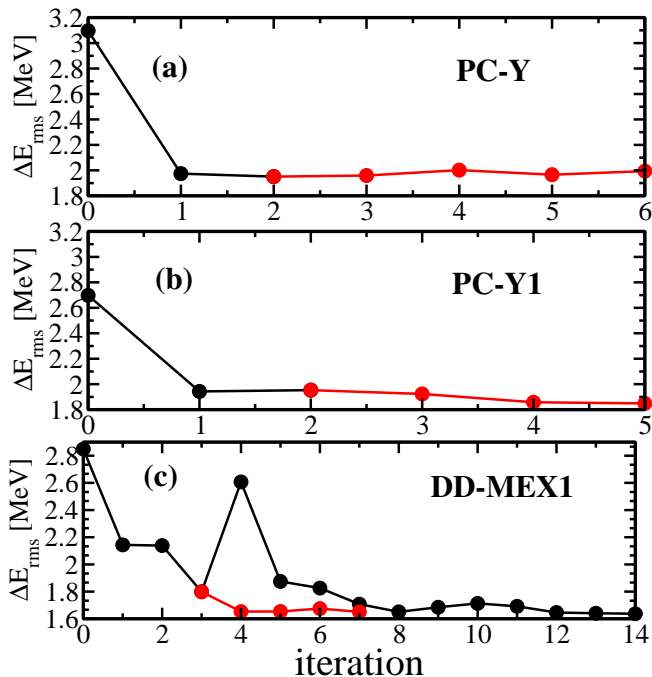


FIG. 1. The evolution of the rms deviations ΔE_{rms} between calculated and experimental binding energies as a function of iteration counter i in the anchor based optimization method for the indicated functionals. Note that ΔE_{rms} is defined for 855 even-even nuclei for which experimental binding energies are known (see Ref. [20] for more details). The steps of iterative procedure for which the correction functions of Eqs. (2) and (20) are used are shown by black and red colors, respectively.

from 200 randomly generated initial points in the large parameter hyperspace at the 0^{th} iteration of ABOA. At subsequent iterations of ABOA the number of randomly generated initial points is decreased to 20 since the parameter hyperspace, which is centered around minimum found at previous iteration and in which the solution is sought, is made smaller.

On average, each minimization of the parameters for 12 spherical anchor nuclei requires approximately 3200 iterations in the optimization process and 8 hours of CPU time are allocated for it⁴. Thus, the total allocated computation time for this step is 12 nuclei times 20 runs times

method (see also Refs. [20, 31]). Note that this number depends on the size of parameter hyperspace. In contrast, the simulated annealing method is extremely costly and numerically unstable for large parameter hyperspaces: in our experience it works reasonably well only in a narrow parameter hyperspace around the global minimum and even then it is by an order of magnitude more time consuming than the simplex method. Note that the simplex method also provides the access to parametric correlations in the functionals (see Ref. [31]).

⁴ The optimization is performed in parallel computer code. Thus, the computation time for each optimization iteration is defined by the nucleus the calculation of which takes the longest time.

8 CPU hours per run which results into 1920 CPU hours for iterations 1, 2, ... of ABOA. Note that computation time allocation is ten times larger for the 0^{th} iteration of ABOA.

The calculations of each of 855 deformed nuclei requires the allocation of 4 CPU hours per run and they are carried out for 4 deformations of basis. This results in the allocation of $855 \times 4 \times 4 = 13680$ CPU hours.

Thus, the 0^{th} iteration and each subsequent iteration of ABOA require the allocation of $19200 + 13680 = 32880$ and $1920 + 13680 = 15600$ CPU hours, respectively. The experience with several types of the functionals tells us that approximately six iterations of ABOA are required to define the functional (see Sec. IV A and Supplemental Material to Ref. [20]). Thus, in total approximately 126400 CPU hours are required for the definition of the functional in the anchor-based optimization. This is only approximately six times more time-consuming than in the typical fitting protocol restricted to 12 spherical nuclei used in Ref. [31] and which corresponds to the optimization of anchor spherical nuclei in the 0^{th} iteration of ABOA.

The next approach is the RGA one. Because of the process of job allocation at HPC², it is possible to calculate maximum 400 nuclei in parallel. The optimization of 400 "spherical" nuclei in the RGA approach is significantly more time consuming than twelve ones in ABOA because of three reasons discussed below. First, the number of "spherical" nuclei is approximately 33 times larger. Second, the CPU time per nucleus in optimization process is significantly larger in the RGA approach than in the ABOA one. This time is defined in parallel calculations by the nucleus the calculation of which takes the longest time since the penalty function is defined at the end of iteration when the information on all nuclei are collected. In that respect, the 12 spherical nuclei used in ABOA are extremely well behaved with fast convergence in numerical calculations in part because the pairing collapses either in one or in both subsystems. In contrast, the pairing is present in most of the nuclei used in the RGA approach and numerical calculations converge slowly in some of these nuclei. Third, because of larger set of nuclei in the RGA approach as compared with ABOA, the optimization of "spherical" nuclei requires larger number of iterations in the minimization process (around 8000) and the allocation of 24 hours per run. Note that similar to ABOA, we use simplex method for minimization with 20 randomly generated initial points in the parameter hyperspace. As a result, one round of optimization of spherical nuclei in the RGA requires $400 \times 20 \times 24 = 192000$ CPU hours.

The calculations of deformed nuclei in the RGA are less numerically costly but they have to be done twice:

This is because the penalty function is defined at the end of each iteration the calculation of which requires the information on each nucleus included in the fitting protocol.

the deformed RHB calculations without constraint on deformation for each nucleus with four initial deformations of basis for the definition of the energy of global minimum and deformed RHB calculations with constraint on spherical shape and with only spherical deformation of basis for the definition of the energy of spherical solutions. Thus the calculational time for deformed nuclei is 400 nuclei times 4 CPU hours per run times 4 runs for different deformations of basis for finding global minima plus 400 nuclei times 4 CPU hours per run for finding spherical solutions; altogether that is 8000 CPU hours.

Thus, one iteration of optimization in the RGA for 400 nuclei requires the allocation of approximately 200000 CPU hours. This is somewhat larger than the time required for defining the functional in the ABOA. If to scale this number to 855 nuclei (as in the ABOA), this would lead to approximately 427500 CPU hours.

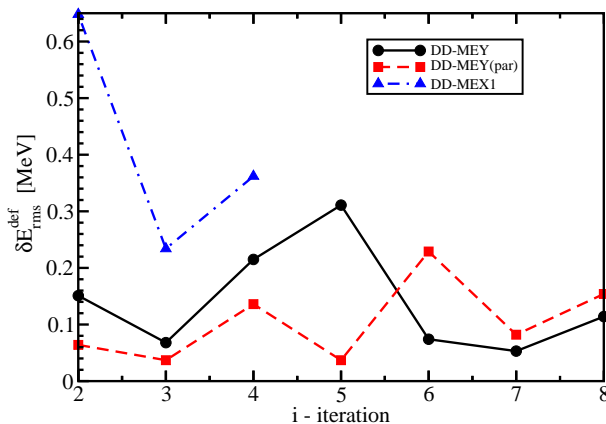


FIG. 2. The convergence of the error in deformation energy in the RGA calculations with indicated functionals. At i -th iteration of the RGA, the deformation energy $E_{def}(Z, N)$ is calculated for the $n = 855$ even-even nuclei using Eq. (1). The error (rms deviation) in deformation energy between the i -th and $(i - 1)$ th iterations of the RGA are then defined as $\delta E_{rms}^{def} = \sqrt{\frac{1}{n} \sum_{k=1}^n [(E_{def})_i(Z, N) - (E_{def})_{i-1}(Z, N)]^2}$.

However, to achieve an optimal solution one should perform a number of iterations of RGA to ensure that the deformation energies E_{def} converge. In order to find how many iterations of RGA are needed for that we carried out the calculations for the CEDFs the fitting protocols of which are the same as for the DD-MEX1 and DD-MEY functionals defined in Ref. [20]. The convergences of the error δE_{rms}^{def} in deformation energies for these functionals are shown in Fig. 2. It was very slow for the DD-MEX1 type of the functional. The best $\delta E_{rms}^{def} = 0.258$ MeV value has been achieved at the 3^d iteration of the RGA (see Fig. 2). However, this value is large and that is a reason why the process has been interrupted after four iterations for this functional. The convergence of the δE_{rms}^{def} errors is better in the DD-MEY type of the functional (see Fig. 2) but even for this functional no full convergence of δE_{rms}^{def} is reached after eight iterations of RGA.

Note that the absence of full convergence of deformation energies affects mostly the nuclei in which the deformation is well pronounced (see Fig. 3). Fig. 2 clearly illustrates that substantial number of additional iterations of RGA would be required for a full convergence of deformation energies. Note that iterative processes shown in this figure were interrupted because of extreme numerical cost: one iteration of RGA is as expensive as a full fit of the functional in ABOA.

It was shown in Refs. [31, 40] that there are correlations between the parameters of state-of-the-art CEDFs: one can speak of parametric correlations between the parameters p_k and p_j when the parameter p_k , with a reasonable degree of accuracy, can be expressed as a function of the parameter p_j . The simplest type of such correlations which exists in CEDFs is a linear one given by

$$f(p_k) = af(p_j) + b \quad (21)$$

where

$$f(p_i) = \frac{p_i}{p_i^{opt}}. \quad (22)$$

Here p_i is the value of the parameter i in the functional variation and p_i^{opt} is the value of the parameter in the optimal functional (see Ref. [31] for detail).

The removing of such correlations allows to reduce the number of free parameters in CEDFs (see Refs. [31, 40]). Here by using the DD-MEY type of the functionals as an example we will evaluate the impact of the removing of parametric correlations on computational time and convergence of deformation energies in RGA. Using the procedure of Ref. [31] one can establish the following correlations between the b_σ , c_ω and c_σ parameters

$$f(b_\sigma) = 0.97303 * f(c_\sigma) + 0.028846, \quad (23)$$

$$f(c_\omega) = 1.14180 * f(c_\sigma) - 0.131090. \quad (24)$$

Thus, the removing of parametric correlations leads to a reduction of the number of free parameters in the DD-MEY type of functionals from 8 to 6. The functional with built-in correlations of Eqs. (23) and (24) is called as DD-MEY(par).

As a consequence of this reduction of the number of adjustable parameters, the time required for one round of optimization of spherical nuclei is reduced by approximately 30%. However, the results labelled as "DD-MEY(par)" in Fig. 2 show that the removing of parametric correlations does not improve substantially the convergence of deformation energies.

Taking all these facts into account one can conclude that RGA is by more than one order of magnitude numerically more time consuming than ABOA and its performance strongly depend on how many iterations of RGA are required for the convergence of deformation energies. However, the latter is strongly dependent on the functional.

FGA approach requires the use of deformed code for the calculations of all nuclei included in the fitting protocol. At present, we did not make any calculations in

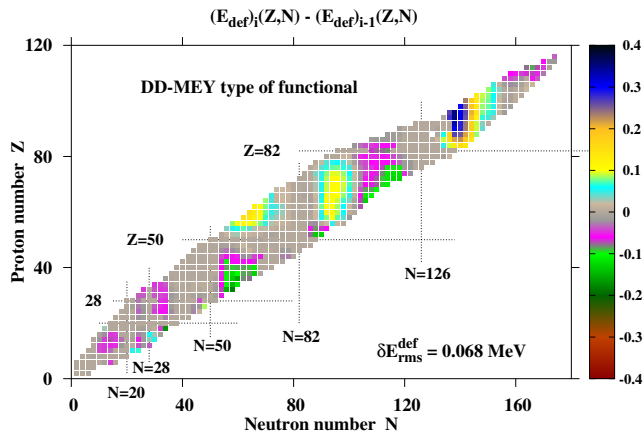


FIG. 3. The distribution of the $(E_{def})_i(Z, N) - (E_{def})_{i-1}(Z, N)$ values across the nuclear chart for the $i = 3$ iteration of the RGA calculations with the DD-MEY type of the functional characterized by $\delta E_{rms}^{def}(Z, N) = 0.068$ MeV (see Fig. 2 and its caption for additional information).

the FGA but a crude estimate can be obtained by comparing the calculational time for the same set of nuclei carried out in spherical and deformed RHB codes. As discussed earlier, the most of numerical cost in the ABOA and RGA calculations are related to the calculations of spherical nuclei. In contrast, the numerical cost in FGA is defined by the cost of the calculations of deformed nuclei. Let us assume that (i) the same set of the nuclei is used in the RGA and FGA and (ii) the number of iterations in the optimization is comparable for the calculations with spherical and deformed RHB codes. Then, the results presented in the columns 4 and 5 of Table II will clearly indicate that the numerical cost of FGA will be larger than that in a single iteration of RGA⁵ by more than three orders of magnitude at fermionic basis with $N_F = 20$ and this cost difference will rapidly increase with increasing N_F .

Note that utilized calculational time is substantially lower than allocated time since many processes finish before the end of allocated time. Utilization rate defined as a ratio of actual calculational time versus allocated one can be improved by a further optimization of the structure of computer codes to the structure of run/time allocation at the HPC². However, in no way it will significantly change the ratio of the computational times of the ABOA, RGA and FGA.

There is an additional issue related to the stability of numerical calculations for the nuclei included into fitting protocol which have not been discussed in the literature on CDFT. The importance of this factor can be illustrated by comparing the parameters of the PC-PK1 and

PC-X functionals in Table 3 of Supplemental Material in Ref. [31]. These two functionals have the same fitting protocols. However, both δ_S and δ_{TV} parameters have opposite signs in these functionals and the penalty function obtained in PC-X is almost by a factor of two better than the one obtained in PC-PK1. A careful analysis reveals that numerical solutions for the pair of very light nuclei included into fitting protocol are unstable at some steps of minimization which in the end leads to non-convergence of the minimization process in a specific volume of parameter hyperspace. Note that this problem has been taken care in the minimization of the PC-X functional by using simplex method starting from large set of randomly generated initial points in the parameter hyperspace. This example clearly indicates that it is beneficial to use in fitting protocols the nuclei in which the numerical solutions behave well. This not only ensures the stability of the minimization process but also enlarges the parameter hyperspace in which the optimum solution can be sought and reduces computational time of minimization. In this respect, a very small set of twelve nuclei included in the fitting protocol of ABOA are extremely well behaved in numerical calculations.

C. DD-MEY functional: ABOA versus RGA

It is important to understand to which extent the ABOA could be a reasonable substitute to a significantly more numerically time-consuming RGA. To do that we carried out RGA calculations using the same experimental information (restricted to binding energies and charge radii) and the isospin-dependent pairing as in the fitting protocol of the DD-MEY CEDF in ABOA (see Ref. [20] for details). The computational procedure discussed in Sec. IV B was used in these calculations.

When comparing the results of the RGA and ABOA calculations one should keep in mind that due to limited computational power the results of the RGA are always a subject of an error δE_{rms}^{def} in deformation energies. However, these errors are acceptable (below 150 keV for δE_{rms}^{def} in considered cases) so that the comparison of these two approaches is feasible. Table VI presents such a comparison between ABOA and RGA results for two iterations of RGA [with respective functionals labelled as DD-MEY(2) and DD-MEY(5)] characterized by δE_{rms}^{def} values of 0.068 and 0.074 MeV, respectively.

One can see that the parameters m_σ , g_σ and g_ω presented in Table VI are very similar for the series of the DD-MEY* functionals obtained in different calculational schemes. Such a localization of these parameters in parameter hyperspace is typical for all functionals which include meson exchange and it is a consequence of the fact that nucleonic potential is defined as a sum of very large attractive scalar S and repulsive vector V potentials (see Refs. [31, 40]). In contrast, other parameters such as g_ρ , b_s , c_s , c_o and a_r in Table VI show somewhat larger relative spreads as compared with m_σ , g_σ and g_ω

⁵ Here we compare full FGA with a single iteration of RGA since FGA does not require the calculation of deformation energies.

TABLE VI. The properties and parameters of indicated functionals. The DD-MEY functional, obtained in ABOA, is taken from Supplemental Material to Ref. [20]. DD-MEY(3) and DD-MEY(6) are the functionals obtained at the 3^d and 6th iterations of the RGA. The global rms deviations $\Delta E_{rms}(\Delta(r_{ch})_{rms})$ between experimental and calculated binding energies (experimental and calculated charge radii) are given by $\Delta E_{rms}(\Delta(r_{ch})_{rms})$. They are defined using all (855 for binding energies and 305 for charge radii) even-even nuclei for which experimental data are available in Refs. [41, 43]. The results for the energy per particle E/A , the density ρ_0 , the incompressibility K_0 , the symmetry energy J and its slope L_0 are displayed in the middle of the table. The parameters of the functionals are presented at the bottom of the table. See text for additional details.

	DD-MEY ABOA	DD-MEY(3) RGA	DD-MEY(6) RGA
1	2	3	4
ΔE [MeV]	1.734	1.672(0.068)	1.725(0.074)
$\Delta(r_{ch})_{rms}$ [fm]	0.0264	0.0294	0.0303
E/A [MeV]	-16.09	-16.044	-16.017
ρ_0 [fm ⁻³]	0.1529	0.1522	0.1545
K_0 [MeV]	265.8	261.6	248.5
J [MeV]	32.8	31.6	30.1
L_0 [MeV]	51.8	42.6	29.5
m_σ [MeV]	551.321796	552.291521	551.989284
g_σ	10.411867	10.398001	10.315743
g_ω	12.803298	12.758552	12.648663
g_ρ	3.692170	3.548208	3.325439
b_s	2.059712	2.249514	2.148238
c_s	3.210289	3.551463	3.464883
c_o	3.025356	3.437551	3.284163
a_r	0.532267	0.652200	0.859341

since for acceptable functionals they are less localized in the parameter hyperspace (see Refs. [31, 40]).

However, considering different sets of the nuclei included in the fitting protocols of RGA (400 nuclei) and ABOA (12 nuclei) and the remaining errors in the deformation energies in the RGA calculations, one can conclude that both ABOA and RGA lead to comparable functionals which provide similar global accuracy of description of binding energies ($\Delta E_{rms} \approx 1.7$ MeV) and charge radii ($\Delta(r_{ch})_{rms} \approx 0.03$ fm) (see Table VI). Note also that the predicted nuclear matter properties (NMP) of these functionals are within the ranges $\rho_0 \approx 0.15$ fm⁻³, $E/A \approx -16$ MeV, $K_0 = 190 - 270$, $J = 25 - 35$ MeV ($J = 30 - 35$ MeV) and $L_0 = 25 - 115$ ($L_0 = 30 - 80$) for the SET2a (SET2b) sets of the constraints on the experimental/empirical ranges for the quantities of interest recommended for relativistic functionals in Ref. [44]. This is the first time that a good reproduction of strict SET2b constraints has been achieved in CDFT by fitting only binding energies and charge radii of finite nuclei: the fitting protocol of DD-MEY* does not contain any

information on NMP (see Supplemental Material to Ref. [20]).

D. Charge radii in ABOA

A general expression for a charge radius r_{ch} in the CDFT is given by [45, 46]⁶

$$r_{ch}^2 = \langle r_p^2 \rangle + r_p^2 + \frac{N}{Z} r_n^2 + \langle r_p^2 \rangle_{SO} + \frac{N}{Z} \langle r_n^2 \rangle_{SO} \quad (25)$$

where $\langle r_p^2 \rangle$ stands for point-proton mean square radius as emerging from the CDFT calculations, r_p and r_n are mean-square charge radii of single proton and neutron, respectively, and $\langle r_p^2 \rangle_{SO}$ and $\langle r_n^2 \rangle_{SO}$ are proton and neutron spin-orbit contributions to the charge radius.

The situation with neutron mean-square charge radius is currently settled: the weighed average of few experiments provides $r_n^2 = -0.1161 \pm 0.0022$ fm² [50] and the value $r_n^2 = -0.1161$ fm² is used in recent studies of charge radii within Skyrme DFT and CDFT frameworks (see Refs. [45, 46, 48]). In contrast, there are some uncertainties in the definition of the proton mean-square charge radius which are generally discussed in the literature as *proton radius puzzle* (see Refs. [51, 52]). This puzzle is known as a discrepancy between proton radius obtained from muonic hydrogen spectroscopy which provides $r_p = 0.8409 \pm 0.004$ fm (see Ref. [50, 52]) and that derived from elastic electron-proton scattering which give a larger value of $r_p = 0.887 \pm 0.012$ fm [51]. It is still not fully resolved and future experiments are required to remove this discrepancy in r_p (see Ref. [52]).

⁶ The analysis of the contributions of the last two terms of this expression in non-relativistic DFTs is presented in Refs. [47–49]. There are some differences between relativistic and non-relativistic treatments of these terms (see detailed discussion in Ref. [46]), however, in general a comparable modification of charge radii is generated by such terms in relativistic and non-relativistic DFTs.

TABLE VII. The rms deviations $\Delta(r_{ch})_{rms}$ between calculated and experimental charge radii r_{ch} for different calculational schemes. See text for more details.

Calculational scheme	DDMEY		NL5(Y)	
	Anchor	Global	Anchor	Global
$r_p = 0.8$ fm				
Scheme-A	0.0143	0.0218	0.0179	0.0294
Scheme-B	0.0162	0.0253	0.0190	0.0308
Scheme-C	0.0186	0.0253	0.0217	0.0308
$r_p = 0.8409$ fm				
Scheme-A	0.0201	0.0241	0.0228	0.0295
Scheme-B	0.0129	0.0223	0.0163	0.0297
Scheme-C	0.0144	0.0223	0.0203	0.0297
$r_p = 0.887$ fm				
Scheme-A	0.0284	0.0291	0.0304	0.0334
Scheme-B	0.0151	0.0217	0.0181	0.0272
Scheme-C	0.0147	0.0217	0.0185	0.0272

To our knowledge all existing CEDFs were fitted with $r_p = 0.8$ fm and only with first two terms in Eq. (25) (see discussion in Ref. [53]): this corresponds to Scheme-A discussed below. Thus, it is important to evaluate the significance of these limitations as well as those connected with proton radius puzzle on the results for the nuclei included in the fitting protocol and on global results. This is done in Table VII which compares the results obtained with three calculational schemes, namely,

- **Scheme-A:** only first two terms of Eq. (25) are included,
- **Scheme-B:** only first three terms of Eq. (25) are included,
- **Scheme-C:** all terms of Eq. (25) are taken into account in the calculations of charge radii of twelve spherical anchor nuclei included in anchor-based optimization. Such results are shown in the columns labelled as "ABOA" in Table VII. In contrast, only three first terms of Eq. (25) are taken into account in the global calculations which also include transitional and deformed nuclei. This is based on the assessment of Ref. [48] that such approximate relation is sufficient in the applications which aim at global description of charge radii⁷. As a result, the global results obtained in Scheme-B and Scheme-C calculations are identical.

⁷ The spin-orbit contribution to charge radii decreases with increasing the mass of nuclei and it almost does not depend on the CEDF. These features are illustrated in Table II of Ref. [45]. Since the calculations of this reference are restricted to spherical shape and neglect the pairing correlations, the values quoted for spin-orbit contribution to charge radii in this table for non-doubly magic nuclei have to be considered as an upper limit. This is because the deformation and pairing give rise to the mixing of different spherical subshells in the structure of the single-particle states which results in a smoothing of the spin-orbit correction to charge radii as a function of particle number [48]. As a consequence, the charge radii in only restricted number of light nuclei

and with three values of $r_p = 0.8, 0.8409$ and 0.887 fm. In addition, the calculations are performed with two CEDFs, namely, DD-MEY and NL5(Y) in order to see the dependence of the results on the functional.

The column "Anchor" of Table VII shows the results for the nuclei included in typical fitting protocol of anchor-based optimization approach (see Ref. [20]) which contains 12 nuclei and only 10 of them, namely, ^{16}O , $^{40,48}\text{Ca}$, ^{90}Zr , $^{116,124,132}\text{Sn}$ and $^{204,208,214}\text{Pb}$ provide the information on charge radii. In the column "Global" we compare the results of the calculations for the set of 261 even-even nuclei in which experimental data on charge radii exist. Note that our set is reduced as compared with the 351 even-even nuclei listed in the compilation of Ref. [43] because of the reasons discussed below. For example, we exclude the nuclei with proton number $Z > 83$ since with the exception of uranium nuclei there are no direct experimental measurements of the absolute charge radii of such nuclei: the data for these nuclei provided in the compilation of Ref. [43] is based on extrapolations. Moreover, we exclude from consideration the nuclei in which beyond mean field and shape coexistence effects have substantial impact on charge radii. These are, for example, the $Z < 10$ nuclei, the Pb and Hg isotopes with $N = 100 - 106$, the Sr, Kr, and Mo isotopes with $N < 50$ (see Ref. [53]). Thus, we focus on the nuclei for which the absolute values of charge radii are experimentally measured⁸ and for which mean field approximation is expected to be a reasonable well justified.

The analysis of the results presented in Table VII leads to the following conclusions. First, the comparisons of the results obtained with $r_p = 0.8409$ fm and 0.887 fm in different calculational schemes clearly indicate that the uncertainties in the value of r_p lead to the uncertainties in rms charge radii. The latter are the largest for calculational Scheme-A in which they are located between 0.0039 fm and 0.0083 fm dependent on the functional and on whether Anchor or Global results are compared. This provides a potential limit on the accuracy with which the charge radii can be meaningfully calculated at present. Further improvement of the description of charge radii below this limit requires the resolution of proton radius puzzle.

Second, Table VII reveals clear correlations between rms deviations $\Delta(r_{ch})_{rms}$ obtained in the Anchor and Global calculations: for a given functional and r_p the calculational scheme with the lowest $\Delta(r_{ch})_{rms}$ value in Anchor calculations provides either the lowest or comparable with the lowest $\Delta(r_{ch})_{rms}$ value in Global calculations. This clearly indicates that the use of twelve

are moderately affected by spin-orbit contributions (see Refs. [45, 46]). Thus, Ref. [48] suggested to ignore last two terms of Eq. (25) in global analysis of charge radii.

⁸ It is sufficient to measure the absolute value of charge radius of a single nucleus in isotopic chain and then to establish the charge radii of other nuclei in the chain by means of laser spectroscopy (see Ref. [54]).

anchor spherical nuclei in ABOA ten of which contain experimental information on charge radii is sufficient for constraining the properties of charge radii globally.

Note that the extension of the dataset of the nuclei with charge radii used in the fitting protocol beyond these ten nuclei will not necessarily improve the agreement with experiment on a global scale because of increased theoretical uncertainties in the description of charge radii of the ground states. Indeed, charge radii sensitively depend on the underlying single-particle structure (see Refs. [53, 55, 56]) the accuracy of the description of which typically reduces on going on from spherical to deformed nuclei (see, for example, Refs. [57–59]). In addition, in the case of the nuclei with shape coexistence or soft potential energy surfaces the beyond mean effects have to be taken into account and their inclusion in model description is extremely numerically costly. Thus, the restriction of the dataset of the nuclei with charge radii used in the fitting protocol to spherical predominantly single and doubly magic ones reduces theoretical uncertainties related to the shape of the nucleus and underlying single-particle structure. However, for these nuclei the inclusion of the last three terms of Eq. (25) is important for further improvement of the functionals.

V. ASYMPTOTIC BEHAVIOR OF THE BINDING ENERGIES: BASIS TRUNCATION EFFECTS

The values of N_F and N_B employed in the RMF+BCS or RHB calculations depend on available computational power [which increases with time] and on the approach of theory group to handling the numerical errors in physical observables. In absolute majority of such calculations, N_B is fixed at 20 since the calculations in bosonic sector of the models are relatively cheap. In contrast, the size of the fermionic basis shows substantial variations and dependence on time of publication, the sophistication of theoretical approach and theory group since the cost of numerical calculations in the RMF+BCS and RHB approaches is mostly defined by this sector.

Let us briefly review truncation schemes of fermionic basis of existing global mass calculations in the CDFT framework. Note that we specify N_B below only if it differs from 20. The $N_F = 12$ value has been used in global RMF+BCS mass calculations with NL3 CEDF in Ref. [60] with a larger number of fermionic shells used in very heavy nuclei. The RMF+BCS calculations of Ref. [61] have been carried with $N_F = N_B = 14$ and TMA CEDF. Global RMF+BCS calculations with CEDFs NL3, TM1, FSUGold and BSR4 were performed in Ref. [62] with $N_F = 18$. $N_F = 20$ was used in global RHB calculations with the DD-ME2, DD-PC1, NL3* and DD-ME δ functionals in Ref. [5]. Ref. [63] presents the results of the global RMF+BCS calculations with phenomenological treatment of the dynamical correlation energy and CEDF PC-PK1: it uses $N_F = 14$ for $Z < 60$ nuclei

and $N_F = 18$ for heavier ones. The transition to microscopic beyond mean field approaches leads to a significant increase of computational time. As a consequence, the fermionic basis is reduced in such studies. For example, the first global investigation within five-dimensional collective Hamiltonian (5DCH) based on triaxial RMF+BCS calculations with PC-PK1 CEDF employs $N_F = 12, 14$ and 16 for the nuclei with $Z < 20$, $20 \leq Z \leq 82$, and $Z \geq 82$, respectively (see Ref. [64]). The same fermionic basis is used in the 5DCH studies based on triaxial RHB calculations with PC-PK1 CEDF presented in Ref. [65].

While the majority of these schemes of the truncation of the fermionic basis provide a sufficient accuracy for absolute majority of physical observables (such as radii, deformations, etc) it is still an open question on how accurate they are for the calculations of the binding energies. This is because the assessment of the accuracy of the truncation of the basis in these publications has been either not carried or performed by comparing the solutions obtained with N_F and $N_F + 2$ (or $N_F + 6$ as in Ref. [5]) for very restricted set of nuclei. As a consequence, a number of the issues has not even been considered in earlier publications. For example, how the truncation errors in binding energies depend on the type of the functional? Or what is the evolution of truncation errors with proton and neutron numbers? Are those errors gradually increase with particle numbers or there are some local fluctuations caused by the shell effects?

To address these questions one should consider an asymptotic limit for the binding energies $B(Z, N)$ ⁹ which corresponds to $N_F \rightarrow \infty$ and $N_B \rightarrow \infty$. The asymptotic (negative) binding energy corresponding to these limits is defined as $B_\infty(Z, N) = B(N_F \rightarrow \infty, N_B \rightarrow \infty)$ and it serves as a benchmark with respect of which the truncation errors in binding energies in the basis with (N_F, N_B) have to be defined. The consideration of this limit and related truncation errors are presented below for bosonic and fermionic sectors separately.

A. Bosonic sector

Since the bosonic basis size grows modestly with N_B the absolute majority of the RMF+BCS and RHB calculations have been performed with $N_B = 20$ starting from 90ites of the last century. For most of physical observables, this basis provides a required accuracy. However, we are not aware of any publication in which the convergence of binding energies as a function of N_B has been presented. Fig. 4 and Table VIII fills this gap in our knowledge and shows the dependence of the difference $\Delta B(N_B) = B(N_B) - B_\infty$ between the calculated binding energies $B(N_B)$ and B_∞ on the number of bosonic

⁹ $B(Z, N)$ is the (negative) binding energy of the nucleus with Z protons and N neutrons.

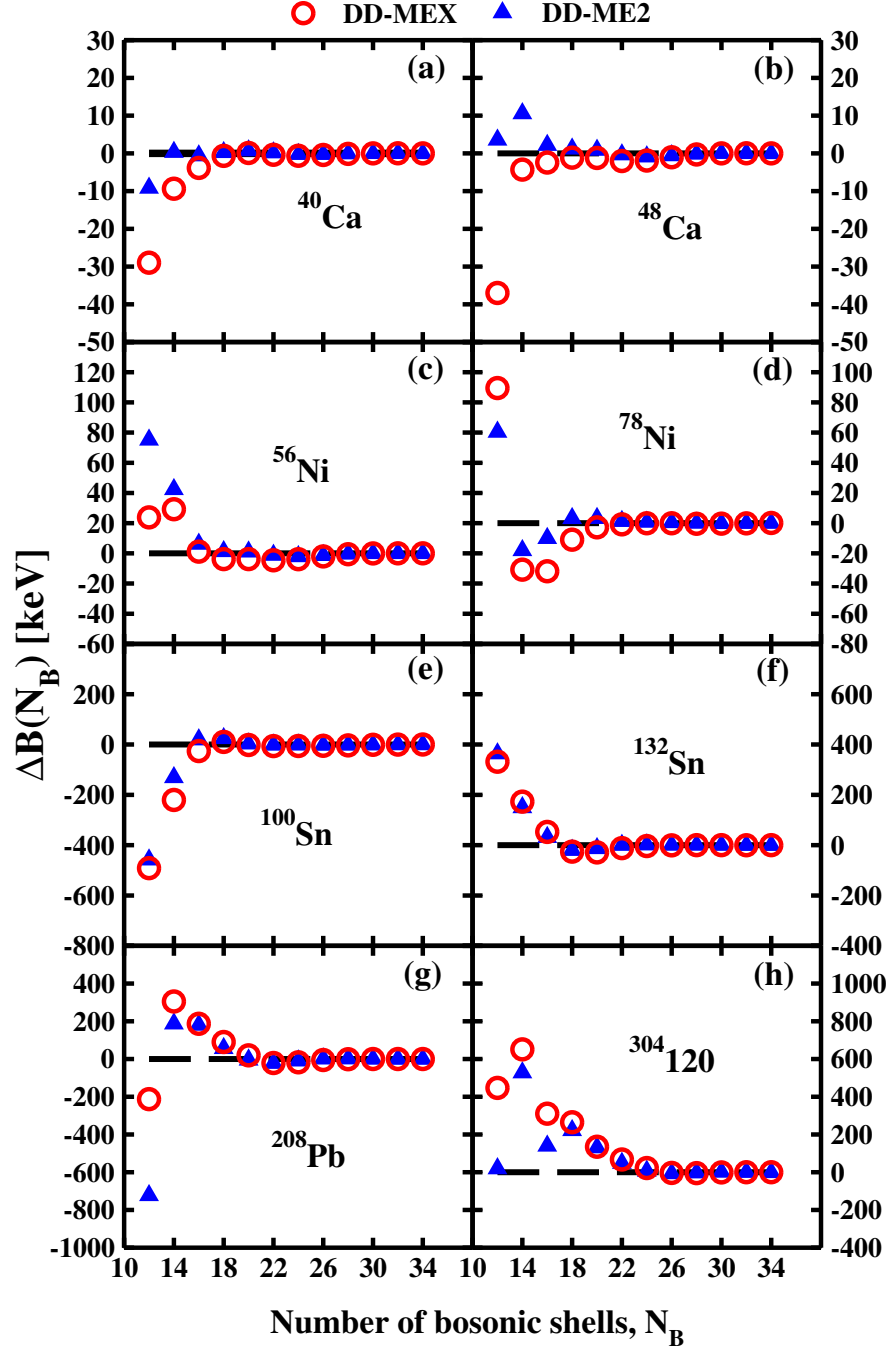


FIG. 4. The dependence of the difference $\Delta B(N_B) = B(N_B) - B_\infty$ on the number of bosonic shells N_B . The asymptotic limit is shown by black dashed line. The $\Delta B(N_B)$ values are shown by blue solid triangles and open red circles for the DD-ME2 and DD-MEX CEDFs, respectively.

shells N_B for selected set of spherical nuclei ranging from light to superheavy ones. The binding energies obtained in the calculations with $N_B = 32$ and $N_B = 34$ do not differ by more than 1 keV both in spherical and deformed calculations. Thus, their average is treated as B_∞ . Note that fermionic basis is fixed at $N_F = 20$ in these calculations. To illustrate the dependence of the convergence of binding energies with increasing N_B on the functional,

the calculations are carried out with for CEDFs DD-ME2 [38] and DDMEX [31], which are similar in structure but somewhat different in numerical values of the parameters.

The convergence pattern of binding energies as a function of N_B depends on the nucleus. For example, the ^{40}Ca and ^{100}Sn nuclei are more bound at low N_B ($\Delta B(N_B) < 0$) as compared with asymptotic limit which they gradually reach with increasing N_B [see Fig. 4(a)

and (e)]. In contrast, the ^{132}Sn nucleus is less bound ($\Delta B(N_B) > 0$) at $N_B \leq 16$ than asymptotic limit, then it becomes slightly more bound for $N_B = 18 - 24$, and finally approaches asymptotic limit [see Fig. 4(f)]. Similar but inverted behavior is seen in ^{78}Ni [see Fig. 4(d)]. If to exclude the results at $N_B = 12$, the ^{208}Pb nucleus is less bound than in asymptotic limit for $N_B = 14 - 20$ but calculated binding energies are close to asymptotic limit at higher N_B [see Fig. 4(g) and (h)].

The convergence of the results to asymptotic limit only weakly depends on the functional [see Table VIII]. Few keV accuracy is achieved globally with $N_B = 28$, in sub-lead ($Z < 82$) region with $N_B = 24$ and in tin and sub-tin ($Z \leq 50$) region with $N_B = 20$. With increasing mass number, the accuracy of a given truncation of bosonic basis decreases. For example, the truncation scheme with $N_B = 20$ is accurate up to 1 keV in ^{40}Ca in both functionals. However, its accuracy drops to ≈ 130 keV in superheavy $^{304}120$ nucleus. Note that the sign of $\Delta B(N_B)$ fluctuates across the nuclear chart for a given N_B : this means that in some nuclei a given truncation scheme provides more bound and in others less bound solutions as compared with asymptotic ones (see also Fig. 4).

The numerical errors in the description of binding energies increase on transition from spherical to deformed nuclei. This is illustrated in Table IX on the example of selected deformed rare-earth, actinide and superheavy nuclei. For example, the use of $N_B = 20, 24$ and 28 in rare-earth ^{162}Sm , ^{164}Dy and ^{170}Yb nuclei leads to ≈ 50 keV, ≈ 10 keV and a few keV errors in the description of binding energies, respectively. These errors somewhat increase on transition to actinides ($^{240,250}\text{Pu}$) and superheavy (^{272}Ds , ^{278}Cn) nuclei so that it is required to use $N_B = 28$ basis to achieve ≈ 10 keV errors in these nuclei. Note that the errors in the light and medium mass ($A < 130$) nuclei which are not shown in Table IX are substantially lower than those in rare-earth region.

Considering the patterns of the behavior of $\Delta B(N_B)$ with increasing N_B shown in Fig. 4 (such as those in ^{132}Sn), the extrapolation relations (similar to those discussed in Sec. VB) based on small size of bosonic basis can suffer from numerical errors. Thus, taking into account the modest increase of basis size with N_B , it is better to use large bases (such as $N_B = 28$) for precise mass calculations. This will lead only to modest increase of computational time and memory requirements as compared with $N_B = 20$ case and can be easily handled on modern high-performance computers.

B. Fermionic sector

1. Binding energies

The asymptotic values of binding energy are extremely numerically expensive to calculate and we are not aware about any attempts in the CDFT framework apart of those presented in Refs. [20, 66] for a few nuclei to obtain

TABLE VIII. The $\Delta B(N_B)$ values (in keV) for $N_B = 20, 24$ and 28 for the CEDF DD-ME2 and DD-MEX.

Nuclei	DD-ME2			DD-MEX		
	$\Delta B(20)$	$\Delta B(24)$	$\Delta B(28)$	$\Delta B(20)$	$\Delta B(24)$	$\Delta B(28)$
^{40}Ca	0.72	-0.24	0.02	0.10	-0.63	-0.14
^{48}Ca	0.90	-0.87	-0.15	-1.23	-1.90	-0.30
^{56}Ni	1.10	-1.99	-0.34	-3.83	-3.90	-0.56
^{78}Ni	3.23	0.72	0.09	-2.79	-0.07	-0.37
^{100}Sn	3.42	-0.95	-1.60	-1.69	-5.65	-3.22
^{132}Sn	-12.74	1.98	0.61	-28.73	-3.42	0.21
^{208}Pb	-4.25	-9.00	2.03	19.58	-17.34	-0.86
$^{304}120$	130.96	6.59	-2.09	135.33	21.95	-4.98

TABLE IX. The same as in Table VIII but for selected set of axially deformed nuclei.

Nuclei	DD-ME2			DD-MEX		
	$\Delta B(20)$	$\Delta B(24)$	$\Delta B(28)$	$\Delta B(20)$	$\Delta B(24)$	$\Delta B(28)$
^{162}Sm	-36.38	2.93	0.85	-48.83	-4.76	0.24
^{164}Dy	-40.53	0.49	0.98	-56.03	-9.89	-0.12
^{170}Yb	-50.78	-1.59	1.59	-53.59	-13.79	0.73
^{240}Pu	-33.94	-25.39	0.00	-0.49	-34.30	-4.40
^{250}Pu	11.48	-10.50	-5.01	35.89	-10.74	-8.79
^{272}Ds	-33.33	-24.17	-11.84	-10.13	-17.70	-16.60
^{278}Cn	-57.37	-11.48	-13.06	-38.33	-6.47	-15.63

or to approach these values by a drastic increase of the basis size beyond the one (typically $N_F = 16 - 20$) used in global calculations of binding energies. To address this issue we carried out the calculations for selected sets of spherical and deformed nuclei, the representative cases of which are discussed below.

The evolution of both the calculated binding energy $B(N_F)$ and the quantity $B_{dif}(N_F)$ [defined below] as a function of number of fermionic shells N_F is considered here. The quantity

$$B_{dif}(N_F) = B(N_F + 2) - B(N_F) \quad (26)$$

provides a more accurate measure of the convergence process since it compares the binding energies in the calculations with N_F and $N_F + 2$. The convergence is reached when $B_{dif}(N_F) \rightarrow 0$ with increasing N_F .

The results of the calculations for the evolution of these quantities with the increase of N_F for a few selected spherical and deformed nuclei are presented in Figs. 5 and 6, respectively. A few general conclusions emerge from the analysis of the results of these calculations.

First, the binding energy can either decrease or increase on approaching its asymptotic value and this process depends on CEDFs. For $N_F \geq 18$, the absolute value of binding energy increases for the functionals which contain point coupling (PC-PK1 and DD-PC1) while it decreases for CEDFs which contain meson exchange (NL5(E), DD-ME2 and DD-MEX). This trend can be disturbed and reversed at lower N_F in medium and heavy mass nuclei [see, for example, Fig. 5(e)] leading to the fluctuations of binding energies at $N_F \approx 18$.

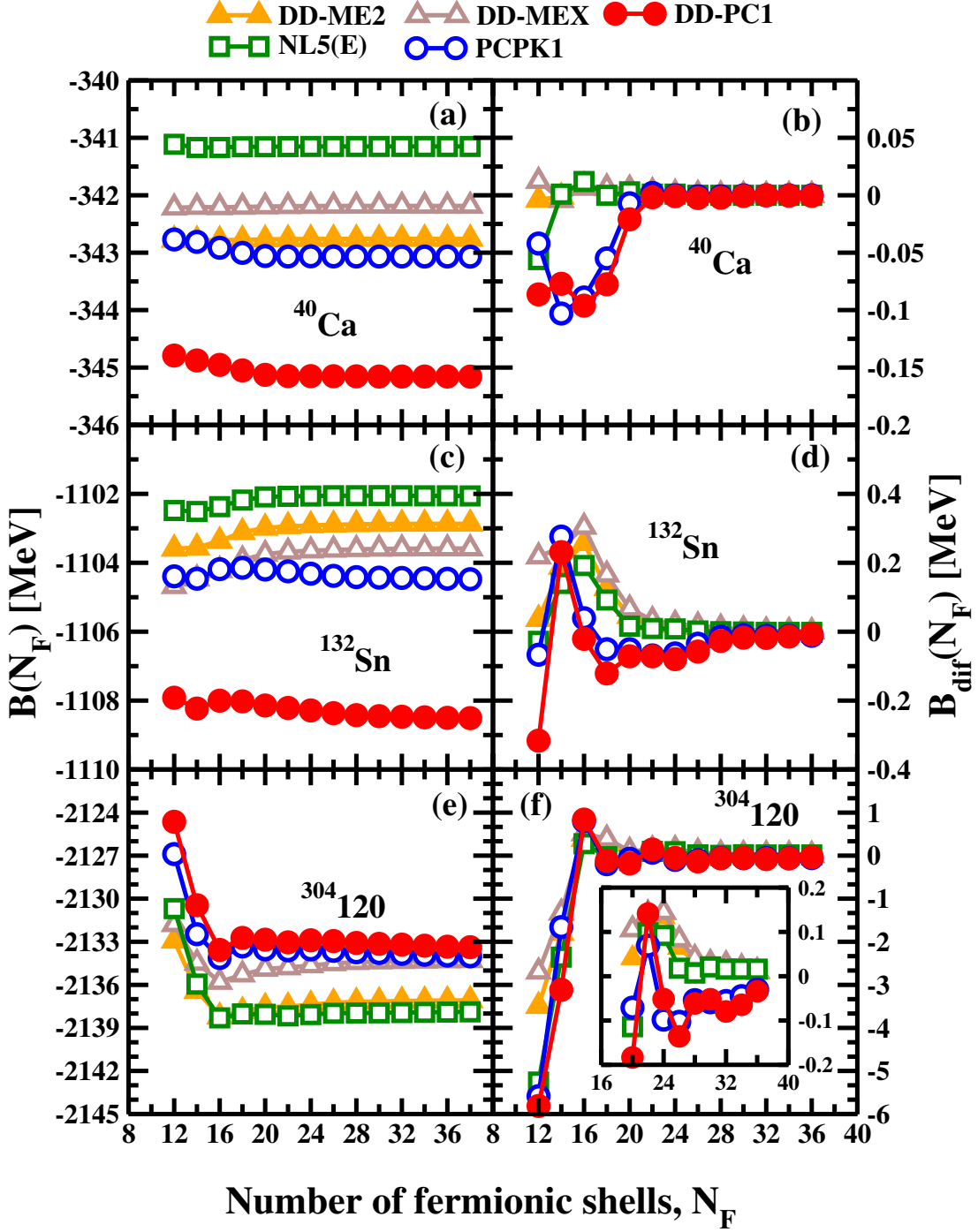


FIG. 5. The evolution of binding energies (left panels) and the $B_{dif}(N_F)$ quantities (right panels) in the ^{40}Ca , ^{132}Sn and $^{304}120$ nuclei under the constraint to spherical shape for indicated functionals.

Second, the convergence speed depends on the functional (see right panels of Figs. 5 and 6). In a given nucleus, the fastest convergence (at lower N_F) is reached by the NL5(E) functional. This follows by the DD-ME2 and DD-MEX functionals which typically require a few extra fermionic shells as compared with NL5(E) for a full convergence. The point coupling functionals are char-

acterized by the slowest convergence since they require additional fermionic shells for a full convergence as compared with the DD-ME* ones. Note that in superheavy $^{304}120$ nucleus no full convergence is reached with PC functionals even with $N_F = 36$ in spherical RHB calculations [see Figs. 5(e)].

Third, the convergence speed depends on the mass of

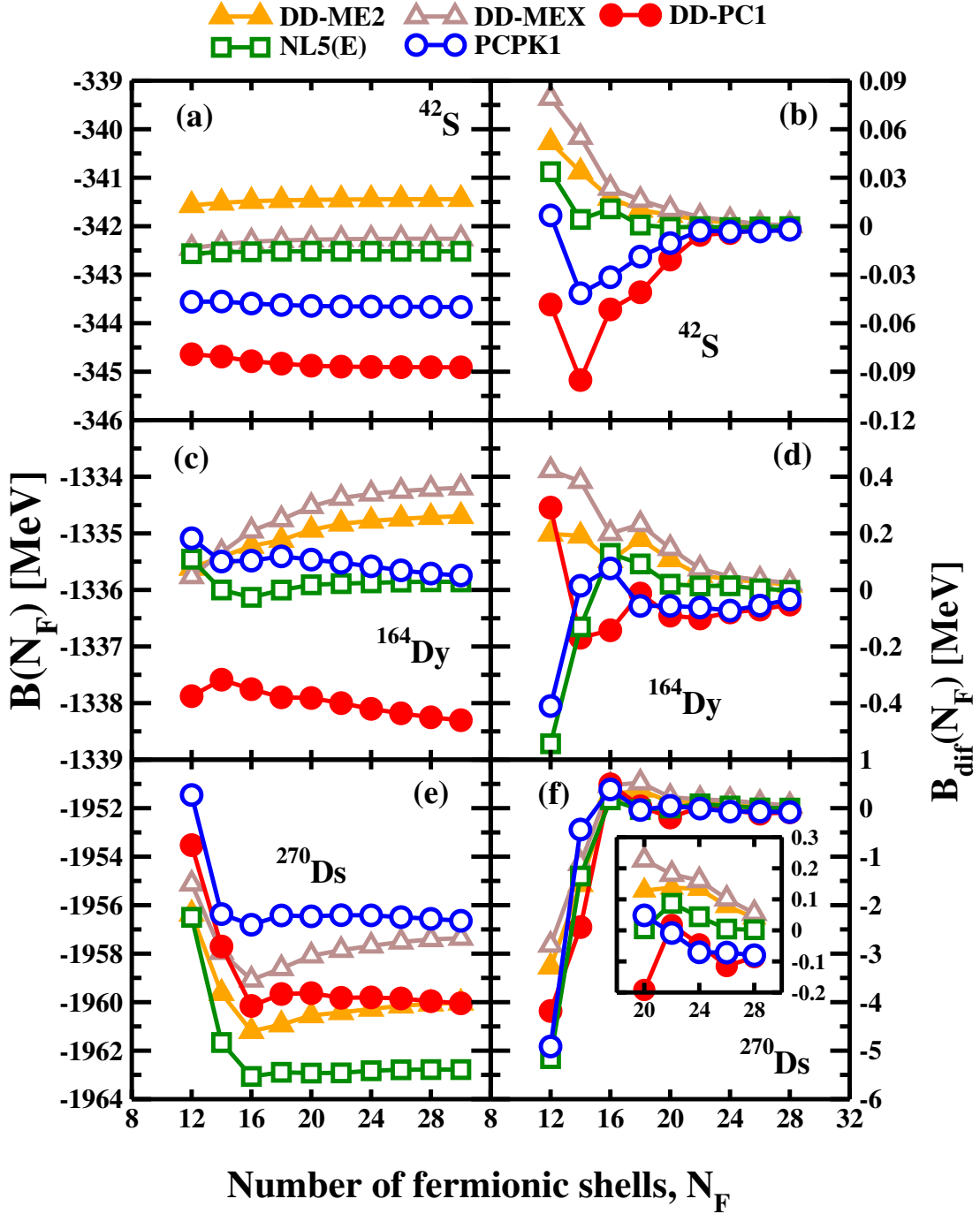


FIG. 6. The same as in Fig. 5 but for deformed ^{42}S , ^{164}Dy and ^{270}Ds nuclei.

the nucleus (see right panels of Figs. 5 and 6). For example, spherical solution converges at $N_F \approx 18$, ≈ 20 and ≈ 22 in the calculations with NLME, DDME and PC functionals in ^{40}Ca [see Figs. 5(b)]. However, to reach a comparable level of convergence one should have $N_F \approx 24$, ≈ 28 and ≈ 36 in ^{132}Sn [see Fig. 5(d)]. The required number of shells increases further for superheavy $^{304}120$ nucleus: the convergent solution is approached at $N_F \approx 26$ in the calculations with NL5(E) functional and

at $N_F = 36$ in the calculations with the DDME functionals [see Fig. 5(f)]. Note that the PC functionals do not fully converge even at $N_F = 36$.

Fourth, some additional increase of the size of fermionic basis is required for a full convergence of the RHB solutions as a function of N_F in deformed nuclei. This is illustrated in Fig. 6. Note that because of the memory allocation limits one can carry out axially deformed RHB calculations only for $N_F \leq 30$. The results

presented in Fig. 6 suggest that the calculations with NL5(E) functional fully converge at $N_F \approx 20$ for masses $A \leq 160$; at $N_F \approx 24$ for masses $160 \leq A \leq 260$ but will require the $N_F > 26$ basis for a full convergence in superheavy nuclei. The DDME functionals require $N \approx 20$, ≈ 26 and ≈ 28 bases for a full convergence in deformed nuclei with masses $A \leq 50$, $50 \leq A \leq 100$ and $100 \leq A \leq 130$, respectively. Higher N_F is required for a full convergence of binding energies in heavier nuclei (see also Sec. VI). The analysis of deformed calculations with the PC functionals confirms that similar to spherical nuclei they require larger fermionic basis for a full convergence as compared with the NLME and DDME ones. Because of the limit of $N_F = 30$ in deformed RHB calculations full convergence of the PC functionals is reached only in light $A \leq 50$ nuclei [see Fig. 6(b)] and its approach is seen in the $50 \leq A \leq 160$ nuclei [see Fig. 6(d)]. However, this size of the basis is not sufficient to judge at which value of N_F the asymptotic value of binding energy will be reached in heavier nuclei [see Fig. 6(f)]. Note that these general conclusions following from the results presented in Figs. 5 and 6 are in line with the ones obtained in the global studies presented in Sec. VI.

It is interesting to compare the convergence of the binding energies as a function of N_F for different nuclei obtained in CDFT with that in non-relativistic DFTs. Unfortunately, to our knowledge such information in latter type of models has been published for only three nuclei, namely, for ^{120}Sn and $^{102,110}\text{Zr}$ in Refs. [24, 25]. The total binding energies of the ^{120}Sn and $^{102,110}\text{Zr}$ nuclei obtained in the Skyrme DFT calculations with the SLy4 force in the basis of $N = 20$ and $N = 25$ HO shells differ by 110-150 keV [24, 25]. Ref. [25] also indicates that the HO basis with $N = 25$ is needed in order to describe the binding energies of the nuclei in this mass region with an accuracy of the couple of tens keV. Tables X and XI show the differences $\Delta B = B(N_F) - B(N_F = 20)$ between binding energies of these three nuclei calculated at N_F and $N_F = 20$ for a few selected values of N_F . One can see that as compared with Skyrme DFT results the convergence of binding energies as a function of N_F is significantly better for the NL5(E) functional, slightly better for the DD-MEX CEDF, and worse for the DD-PC1 one.

Thus, the convergence of binding energies as a function of the basis size is in general comparable for these nuclei in the covariant and Skyrme DFTs. Note that in CDFT the nucleonic potential (≈ -50 MeV/nucleon) emerges as the sum of very large attractive scalar S ($S \approx -400$ MeV/nucleon) and repulsive vector V ($V \approx 350$ MeV/nucleon) potentials [22]. In the nucleus with mass A , these values are multiplied by A and this leads to a cancellation of very large quantities. This is quite different from the structure of the Skyrme DFT [67]. However, this difference in the structure on the models does not have a significant impact on the convergence of binding energies.

TABLE X. The difference $\Delta B = B(N_F) - B(N_F = 20)$ between binding energies of spherical ^{120}Sn nucleus calculated at N_F and $N_F = 20$ for indicated CEDFs.

N_F	ΔB [MeV]		
	DD-MEX	DD-PC1	NL5(E)
24	0.065	-0.137	0.006
26	0.076	-0.201	0.006
30	0.091	-0.284	0.005
38	0.097	-0.318	0.005

TABLE XI. The same as Table X but for deformed $^{102,110}\text{Zr}$ nuclei.

N_F	^{102}Zr : ΔB [MeV]			^{110}Zr : ΔB [MeV]		
	DD-MEX	DD-PC1	NL5(E)	DD-MEX	DD-PC1	NL5(E)
24	0.077	-0.129	-0.015	0.035	-0.118	-0.033
26	0.092	-0.176	-0.017	0.031	-0.165	-0.037
30	0.101	-0.229	-0.022	0.028	-0.215	-0.040

2. Asymptotic values of binding energies: the analysis of the procedure from non-relativistic DFTs.

To circumvent the numerical problem of finding B_∞ in very large basis it was suggested in non-relativistic DFT calculations to use the following approximation [68]

$$B_\infty \approx 2B(N_F + 2) - B(N_F) \quad (27)$$

to estimate the asymptotic value of the binding energy¹⁰ B_∞ . It follows from the following relation

$$[B(N_F + 2) - B(N_F)] \approx 2 \times [B(N_F + 4) - B(N_F + 2)] \quad (28)$$

which was tested in numerical HFB calculations of various nuclei with Gogny D1S force [68]. For example, the prescription of Eq. (27) was used in the fitting protocols of the D1M [18] and D1M* [26] Gogny EDFs and the BCPM functional [13]. However, the numerical accuracy of this approximation has not been defined in either publication.

Note that such an approach has not been used in the CDFT calculations of binding energies so far. In addition, no detailed and systematic numerical analysis of this approach to the calculations of B_∞ and its numerical errors has been published so far in non-relativistic DFTs. Thus, it is important to understand whether this approach works in CDFT and what are related numerical errors.

It turns out that Eqs. (28) and (27) can be easily reduced to

$$B_{dif}(N_F) \approx 2B_{dif}(N_F + 2) \quad (29)$$

¹⁰ Note that in non-relativistic calculations only the number N of harmonic oscillator shells is defined because of the absence of bosonic sector. It is equivalent to N_F in relativistic DFT calculations. Thus the discussion of non-relativistic results is presented here in terms of N_F .

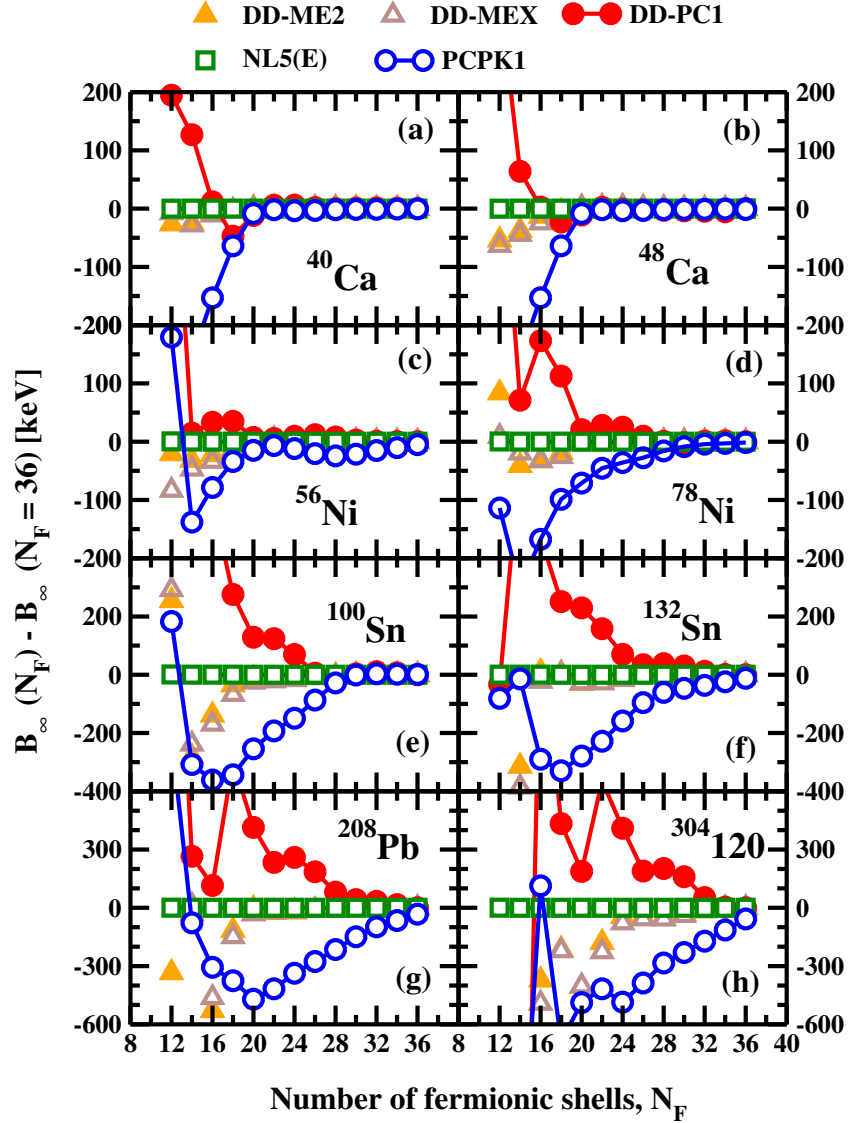


FIG. 7. The dependence of the $B_\infty(N_F) - B_\infty(N_F = 36)$ quantity on the number of fermionic shells N_F . The asymptotic limit is shown by black dashed line.

and

$$B_\infty \approx B(N_F) + 2B_{dif}(N_F), \quad (30)$$

respectively, and the discussion of numerical accuracy of the approximations under consideration can be reduced to the analysis of the evolution of $B_{dif}(N_F)$ with increasing N_F .

Figs. 5 and 6 show the evolution of $B_{dif}(N_F)$ with N_F in selected set of spherical and deformed nuclei, respectively. One can see in the left panels of these figures that in general $B_{dif}(N_F)$ does not follow the rules defined by Eq. (29). Moreover, there are some local fluctuations in B_{dif} at some low to medium values of N_F for some functionals [see Figs. 5(b),(d) and (f) and Figs. 6(b),(d) and (f)] and some drastic changes in the slope of $B_{dif}(N_F)$ in superheavy nuclei at $N_F \approx 16$ [see Figs. 5(f) and Figs.

6(f)].

These results suggest that in reality B_∞ as defined by Eq. (27) [or alternatively, by Eq. (30)] depends on N_F : thus, further we will denote it as $B_\infty(N_F)$. In order to illustrate its dependence on N_F the $B_\infty(N_F) - B_\infty(N_F = 36)$ quantity is shown as a function of N_F for selected set of spherical nuclei in Fig. 7. Since $B_\infty(N_F = 36)$ is very close to asymptotic value of binding energy, the $B_\infty(N_F) - B_\infty(N_F = 36)$ quantity is a measure of numerical error in B_∞ due to the use of finite N_F . In addition, Tables XII and XIII show the numerical values of this quantity at $N_F = 16, 20$ and 36 for the DD-MEX and DD-PC1 CEDFs and compare them with the binding energies calculated at $N_F = 38$.

Based on the results presented in these figures and tables one can make the following conclusions. First, the

TABLE XII. Asymptotic values of binding energy $B_\infty(N_F)$ for a set of spherical nuclei defined at the values of $N_F = 16, 20$ and 36 using prescription defined in Sec. VB2. Column 5 shows the binding energies $B(N_F = 38)$ obtained in the calculations with $N_F = 38$. Note that these values are rounded at 0.1 keV. The calculations are performed with CEDF DD-MEX. The differences $B_\infty(N_F) - B(N_F = 38)$ are shown in the parantheses in columns 2-4.

Nuclei	$B_\infty(N_F = 16)$ [MeV]	$B_\infty(N_F = 20)$ [MeV]	$B_\infty(N_F = 36)$ [MeV]	$B(N_F = 38)$ [MeV]
1	2	3	4	5
^{40}Ca	-342.1970 (-0.0111)	-342.1856 (0.0030)	-342.1860 (-0.0001)	-342.1859
^{48}Ca	-415.2169 (-0.0246)	-415.1901 (0.0022)	-415.1924 (-0.0001)	-415.1923
^{56}Ni	-483.6935 (-0.0343)	-483.6593 (-0.0001)	-483.6598 (-0.0004)	-483.6592
^{78}Ni	-641.2669 (-0.0325)	-641.2364 (-0.0020)	-641.2346 (-0.0002)	-641.2344
^{100}Sn	-828.6610 (-0.1600)	-828.5256 (-0.0246)	-828.5001 (0.0009)	-828.5010
^{132}Sn	-1103.6085 (-0.0224)	-1103.6138 (-0.0277)	-1103.5859 (0.0002)	-1103.5861
^{208}Pb	-1638.1732 (-0.4591)	-1637.7423 (-0.0282)	-1637.7112 (0.0290)	-1637.7141
$^{304}120$	-2134.7740 (-0.4803)	-2134.6843 (-0.3906)	-2134.2822 (0.0115)	-2134.2937

TABLE XIII. The same as Table XII but for the DD-PC1 functional.

Nuclei	$B_\infty(N_F = 16)$ [MeV]	$B_\infty(N_F = 20)$ [MeV]	$B_\infty(N_F = 36)$ [MeV]	$B(N_F = 38)$ [MeV]
1	2	3	4	5
^{40}Ca	-345.1465 (0.0111)	-345.1697 (0.0121)	-345.1581 (0.0050)	-345.1576
^{48}Ca	-418.0405 (0.0049)	-418.0542 (-0.0089)	-418.0431 (0.0022)	-418.0453
^{56}Ni	-481.5399 (0.0322)	-481.5659 (0.0062)	-481.5732 (-0.0011)	-481.5721
^{78}Ni	-645.8577 (0.1720)	-646.0103 (0.0194)	-646.0309 (-0.0012)	-646.0297
^{100}Sn	-827.4990 (0.5906)	-827.9659 (0.1237)	-828.0948 (-0.0052)	-828.0896
^{132}Sn	-1108.0432 (0.4649)	-1108.2864 (0.2217)	-1108.5157 (-0.0076)	-1108.5081
^{208}Pb	-1640.4863 (0.0940)	-1640.1875 (0.3920)	-1640.6014 (0.0211)	-1640.5803
$^{304}120$	-2131.8989 (1.4768)	-2133.2219 (0.1538)	-2133.4097 (-0.0340)	-2133.3757

B_∞ quantity as defined by Eqs. (27) and (30) indeed depends on N_F and this dependence is especially pronounced at low N_F values. For example, the use of the $N_F = 16$ introduces into B_∞ the numerical error of the order of 500 keV for the ^{208}Pb and $^{304}120$ nuclei in the calculations with the DDME functionals [see Figs. 7(g) and (h) and Table XII]. The errors are smaller for lighter nuclei. In reality, the evolution of these numerical errors in B_∞ with N_F is similar to those in binding energies. The numerical errors in B_∞ in general decrease with increasing N_F but there are some local fluctuations in some nuclei which disturb this general trend. For example, in the calculations with DD-PC1 for the $^{304}120$ nucleus the $B_\infty(N_F) - B_\infty(N_F = 36)$ quantity is equal to approximately 200 keV at $N_F = 20$ but it increases to ≈ 700 keV at $N_F = 22$ and then more or less gradually decreases with increasing N_F [see Fig. 7(h)].

Second, the convergence of B_∞ with N_F strongly depends on the functional. It turns out that as a function of N_F , the B_∞ quantity fully converges at lower N_F for the DDME functionals than for the DD-PC1 one. For example, in ^{132}Sn a full convergence (within a few keVs of the $N_F = 36$ results) of the DD-MEX and DD-ME2 functionals is reached at $N_F = 26$, while to achieve that in the DD-PC1 functional one should have $N_F = 34$ [see Fig. 7(f)].

Third, Fig. 7 and Tables XII and XIII clearly illustrate that for a given functional the size of fermionic basis required for a full (or nearly full) convergence increases with mass number of the nucleus.

3. Global comparison of binding energies at different truncation of fermionic basis.

Fig. 8 provides a global comparison of the differences of binding energies obtained in the calculations with $N_F = 16, N_F = 20$ and $N_F = 30$. The first two truncations of the fermionic basis were frequently used in the RHB and RMF+BCS calculations during the last decade, and the last one is the maximum achievable in the deformed RHB calculations at high-performance computing facility used by our group.

One can see in Fig. 8 that local fluctuations in the $B(N_F = 20) - B(N_F = 16)$ values are quite substantial in some parts of the nuclear chart. Moreover, these fluctuations can have different signs in different parts of the nuclear landscape. For example, for the NL5(E) CEDF the rare-earth and superheavy nuclei are less bound and the nuclei in lead region and actinides are more bound in the calculations with $N_F = 20$ than those in the calculations with $N_F = 16$ [see Fig. 8(a)]. However, the absolute values of $B(N_F = 20) - B(N_F = 16)$ very rarely exceed 0.3 MeV. In contrast, the $Z > 20$ nuclei are less bound in the $N_F = 20$ calculations with DD-MEX functional and the $B(N_F = 20) - B(N_F = 16)$ difference increases with increasing mass number reaching the vicinity of 1.0 MeV in actinides and superheavy nuclei [see Fig. 8(c)]. However, the $B(N_F = 20) - B(N_F = 16)$ difference is not a smooth function of mass or particle numbers since substantial local deviations from a general trend are present [see Fig. 8(c)]. For the DD-PC1 and PC-PK1 functionals,

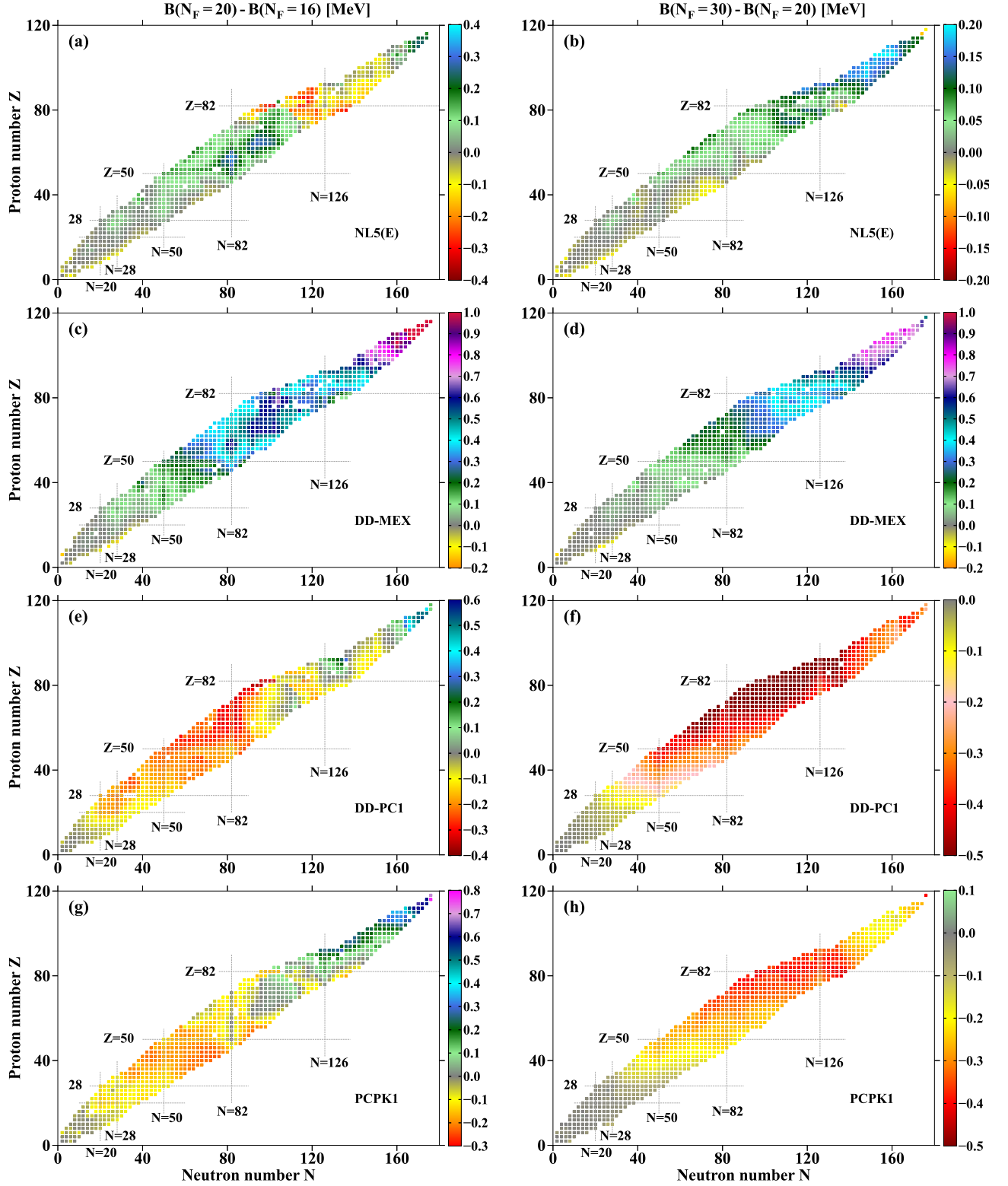


FIG. 8. The difference between binding energies $B(N_F) - B(N'_F)$ calculated with indicated truncations of the fermionic basis for the 855 even-even nuclei for which experimental data exists in Ref. [41]. White squares are used for the nuclei in which the calculations with compared truncations of the basis bring the quadrupole deformations β_2 which differ by more than 0.01. Note that the colormaps are different in different panels.

the nuclei located between neutron numbers $N \approx 20$ and $N \approx 90$ are more bound in the calculations with $N_F = 20$ [see Fig. 8(e) and (g)]. In contrast heavier nuclei are typically less bound and this trend is more pronounced in the PC-PK1 functional. In addition, local fluctuations in the $B(N_F = 20) - B(N_F = 16)$ values are seen for the $N \geq 90$ nuclei and they are somewhat more pronounced in the calculations with DD-PC1.

The $B(N_F = 30) - B(N_F = 20)$ values behave significantly smoother as a function of particle number than the $B(N_F = 20) - B(N_F = 16)$ ones (compare right with left panels in Fig. 8). This clearly suggest that the local fluctuations seen in the $B(N_F = 20) - B(N_F = 16)$ values are due to the impact on underlying shell effects on the convergence of binding energies as a function of N_F which is significantly more pronounced at low value of $N_F = 16$.

In all studied functionals the $B(N_F = 30) - B(N_F = 20) \approx 0$ in light nuclei (see Fig. 8). However, with increasing mass number the nuclei gradually become less and less bound in the NL5(E) and DD-MEX functionals and the $B(N_F = 30) - B(N_F = 20)$ values gradually approach ≈ 0.2 and ≈ 1.0 MeV in superheavy nuclei, respectively [see Fig. 8(b) and (d)]. The situation in the calculations with PC functionals is different: the nuclei located between proton numbers $Z \approx 40$ and $Z \approx 90$ are more bound (by up to 0.5 MeV) in the calculations with $N_F = 30$ than those in the calculations with $N_F = 20$ but that difference decreases on moving away from this region [see Figs. 8(f) and (h)].

VI. ASYMPTOTIC VALUES OF BINDING ENERGIES: ALTERNATIVE PROCEDURE.

The detailed analysis of the prescription for finding asymptotic value of binding energy in the modest size basis which is used in non-relativistic DFTs presented in Sec. VB2 clearly indicates that this method does not provide high numerical accuracy and predictive power in the case of CDFT. Thus, an alternative procedure is required.

We suggest to base this procedure on the analysis of the evolution of B_{dif} as a function of the number of fermionic shells N_F . The typical patterns of such evolution are shown in Fig. 9. The full convergence of the calculated binding energies as a function of N_F is reached when $B_{dif} = 0$. Blue dot dashed lines labeled as C in Figs. 9(a) and (c) show linear interpolations for B_{dif} obtained based on the points at $N_F = 16$ and $N_F = 18$. One can see that linear extrapolations based on these interpolations will lead to divergent results. The use of the data points at $N_F = 18, 20$ and 22 in the case of the ^{42}S and ^{132}Sn nuclei and $N_F = 18 - 24$ in the case of ^{164}Dy leads to the red dashed interpolation lines labelled as B in Fig. 9. One can see that linear extrapolations based on these interpolations will lead to convergent results for binding energies in the cases of the ^{42}S and ^{132}Sn nuclei

but to divergent results in the case of the ^{164}Dy nucleus. Finally, the linear interpolations obtained based on the $N_F = 22 - 28$ data points in the cases of the ^{42}S and ^{132}Sn nuclei and with $N_F = 24 - 28$ in the case of the ^{164}Dy nucleus are shown by thick solid black lines labelled as A in Fig. 9. One can see that numerical results fully converge in the first two nuclei and show approach of full convergence (which according to linear extrapolation is expected around $N_F \approx 31$) in ^{164}Dy .

The absence of a unique smooth convergence pattern of B_{dif} as a function of N_F and the drastic changes of their slopes at some values of N_F which are seen in the change of the slopes of the interpolations C, B and A in Fig. 9 clearly indicate that the information on binding energies for $N_F > 20$ is needed in order to have a numerical accuracy of calculated binding energies within a few tens of keV. Thus the following calculational scheme for the definition of asymptotic binding energies is suggested and used in the present paper:

- The global calculations for binding energies of all nuclei included into fitting protocol are performed in deformed RHB code with $N_F = 20, 22, 24, 26, 28$ and 30 . This¹¹ is done after several initial steps of the optimization of the functional with $N_F = 20$ when the global rms deviations between experimental and calculated binding energies reach 2–3 MeV. This guarantees that the corrections for binding energies between $N_F = 20$ and $N_F = \infty$ bases are almost the same for this somewhat non-optimal solution and the optimal one¹². As a consequence, such calculations for corrections in binding energies have to be done only once.
- The results of such calculations allow to define $B_{dif}[Z, N](N_F)$ for each nucleus included into the

¹¹ Although such calculations are numerically expensive (see Table I), they are feasible at modern high-performance computers. The computational time presented in this table can be further reduced by at least 30% if the calculations at N_F are carried from the fields defined at $N_F - 2$. Note that the data presented in Table I has been obtained in numerical calculations starting from the fields given by the Woods-Saxon potential to guarantee the same initial conditions. An extra time required for such calculations of the 855 nuclei ranges from approximately 15000 CPU-hours for the DD-PC1 functional to approximately 21000 CPU-hours for the DD-MEX one (the numbers are based on the data of Table I). This is less than 10% of the calculational time of full ABOA and one iteration in the RGA.

¹² This expectation is based on the fact that the evolution of B_{dif} with N_F in a given nucleus is very similar for the functionals representing the same class of CEDFs. For example, the analysis of right panels in Figs. 5 and 6 clearly shows that this is a case for the DD-ME2 and DD-MEX functionals which represent the DD-ME* class of the functionals and for the DD-PC1 and PC-PK1 CEDFs which are representative examples of the PC functionals. This clearly indicates that for a given class of the functionals the variations of the parameters of the functional within a reasonable range do not affect substantially the convergence of binding energies as a function of N_F .

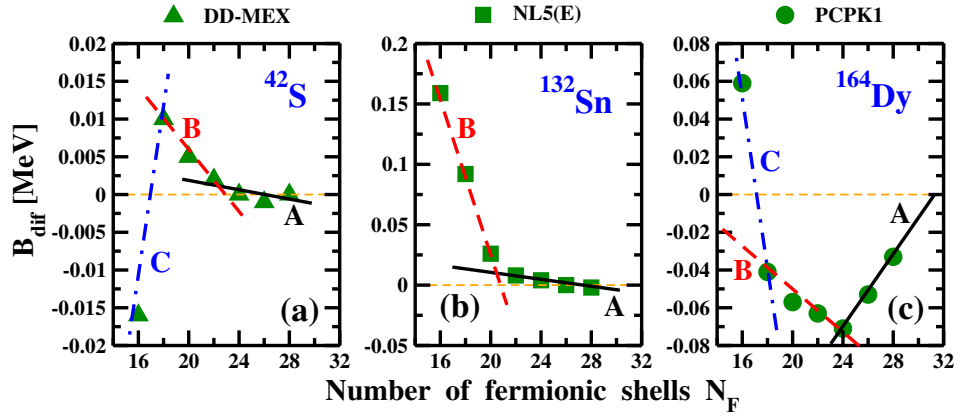


FIG. 9. Typical patterns of the evolution of B_{dif} as a function of the number of fermionic shells N_F illustrated by a few selected cases. They are based on the analysis of the results of the calculations for a significant number of nuclei, the small part of which is presented in Figs. 5 and 6. Thin orange dashed lines show $B_{dif} = 0$. Thick blue dot-dashed, red dashed and black solid lines show the interpolations of the evolution of B_{dif} on the subsets of calculated data points. See text for further details. The employed functionals are indicated.

fitting protocol and consequently the infinite basis correction $\Delta B_\infty(Z, N) = B[Z, N](N_F = 20) - B[Z, N](N_F = \infty)$ using the following procedure:

- (A) The infinite basis correction is equal to $\Delta B_\infty(Z, N) = B[Z, N](N_F = 20) - B(Z, N)(N_F = 30)$ for the cases when (i) $B_{dif}[Z, N](N_F) \leq \delta E_{err}$ for $N_F = 28, 26$ and 24 and (ii) the linear interpolation of $B_{dif}[Z, N](N_F)$ based on these N_F [see line A in Figs. 9(a) and (b)] clearly indicates the convergence of calculated binding energies. Here the δE_{err} [defined by the user - typically a few keV] is related to the error in the definition of the value of asymptotic binding energy.
- (B) In the cases when B_{dif} clearly shows the trend of the convergence of binding energies with increasing N_F [as for the interpolation line A in Fig. 9(c)] the convergence point at \tilde{N}_F is defined by linear extrapolation of the interpolation line defined at $N_F = 24, 26$ and 28 to $B_{dif} = 0$ [i.e. $B_{dif}(\tilde{N}_F) = 0$]. This allows to define extrapolated energy $B(\tilde{N}_F)$, which is associated with infinite basis binding energy $B_\infty(Z, N) = B(\tilde{N}_F)$, and infinite basis correction $\Delta B_\infty(Z, N) = B[Z, N](N_F = 20) - B[Z, N](\tilde{N}_F)$.
- If the conditions given in (A) and (B) are not satisfied [as for interpolation line B in Fig. 9(c)], this means that full convergence of B_{dif} cannot be defined at $N_F = 30$. This is typically happening in the PC models for very heavy nuclei (see discussion below). To define $\Delta B_\infty(Z, N)$ for such cases one should carry the numerical calculations at the N_F values which are beyond $N_F = 30$.

Such procedure allows to define the map in the (Z, N) plane of the infinite basis corrections which can be used at all iterations of the fitting procedure. In addition, it allows to evaluate the numerical errors in the definition of such corrections.

The infinite basis binding energies $B_\infty(Z, N)$ obtained with discussed above procedure are compared with those obtained in the calculations with $N_F = 20$ and $N_F = 30$ in Fig. 10. The analysis of this figure reveals some important features.

First, the infinite basis binding energies can be defined for the NL5(E) and DD-MEX functionals for all nuclei of interest. In contrast, in the case of the DD-PC1 and PCPK1 functionals, they can be defined only for sub-lead region and for some nuclei which have spherical shape in lead and superheavy region. Note that the definition of B_∞ for latter nuclei is done in spherical RHB code which allows the calculations with $N_F = 38$. To define B_∞ for the PC functionals for transitional and deformed nuclei in the lead region, actinides and superheavy region one should carry out numerical calculations in deformed RHB code with $N_F > 30$ which are numerically impossible at present. However, based on the examples of the DD-MEX functional [see Figs. 10(c) and (d)] and PC functionals for $Z < 80$ region [see Figs. 10(e), (f), (g) and (h)], it is reasonable to expect that infinite basis corrections $\Delta B_\infty(Z, N)$ for the deformed and spherical nuclei in the regions under discussion will be comparable and will not differ by more than 100-200 keV also for the PC functionals.

Second, the results presented in the right column of Fig. 10, which compares the $B(N_F = 30)$ and B_∞ values, show that the NL5(E) CEDF is characterized by the best convergence among considered functionals. Indeed, only in a few nuclei the absolute value of $B_\infty - B(N_F = 30)$ exceeds 10 keV [see Fig. 10(b)]. The next best convergence is obtained for the DD-MEX functional for which

the $B_\infty - B(N_F = 30)$ stays below 100 keV even in superheavy nuclei [see Fig. 10(d)]. In contrast, the worst convergence is obtained for the functionals which contain point coupling: some heavy nuclei in the infinite basis are more bound than the ones in the $N_F = 30$ basis by around 500 keV and 150 keV in the DD-PC1 and PC-PK1 functionals, respectively. In addition, no B_∞ values can be defined for actinides and superheavy nuclei in deformed RHB calculations with $N_F \leq 30$. These features are rather general: the analysis of other less systematic calculations reveals that the best convergence as a function of N_F is obtained in the simplest class of the functionals, namely, NLME one, followed by the DDME CEDFs and the worst convergence exist in the PC functionals. The analysis of the structure of the functionals suggests that the addition of derivative terms to the functional makes convergence of the functional as a function of N_F worse.

Third, the analysis of the results presented in the left column of Fig. 10 clearly illustrates that on average the $B_\infty - B(N_F = 20)$ values evolve reasonably smoothly with increasing mass number. Note that the fits of many CEDFs carried out within the last two decades are performed in the $N_F = 20$ basis. For such functionals the part of the effects related to the truncation of the basis seen in the smooth trend of the evolution of the $B_\infty - B(N_F = 20)$ values with mass number is built into the model parameters during the fitting procedure¹³. However, some local fluctuations and isospin trends seen in the $B_\infty - B(N_F = 20)$ values are not taken care in such an approach. To resolve them the mapping of the binding energies to infinite basis is needed. This can be done by mapping infinite basis corrections $\Delta B_\infty(Z, N)$ and using them in the fitting protocol which is based on the $N_F = 20$ basis. These corrections are expected to be only marginally affected by the local variations of the parameters of the functional and thus their map in the (Z, N) plane can be calculated only once.

Relative errors in the calculations of the binding energies in the $N_F = 20$ basis as compared with infinite basis binding energies are presented in Fig. 11. For absolute majority of the nuclei they are better than 0.05%. The impact of the transition from the basis with $N_F = 20$ to the infinite basis is very small and below experimental uncertainties for other physical observables such as deformations, single-particle energies, moments of inertia etc. This is a reason why the $N_F = 20$ basis is sufficient for the calculations of such physical observables. The only exceptions are few transitional or shape-coexisting nuclei (shown by white squares in Fig. 11) in which such

a transition triggers either moderate change of deformation because of softness of potential energy surface or the transition from one to another minimum in potential energy surface. For such nuclei, infinite basis correction $\Delta B_\infty(Z, N)$ can be defined as an average of such corrections in neighboring nuclei.

VII. CONCLUSIONS

The main goal of the present study is further development of covariant energy density functionals towards more accurate description of the binding energies across the nuclear chart. It is focused on detailed analysis of the anchor based optimization approach (ABOA), its comparison with alternative global fitting protocols and on the global analysis of the errors related to the truncation of bosonic and fermionic bases in the calculation of binding energies and on the design of new fitting protocols which will allow to eliminate such errors. The main results of this study can be summarized as follows.

- The detailed comparison of the anchor based optimization approach (ABOA) of global optimization of energy density functionals with fully global (FGA) and reduced global (RGA) approaches has been presented. The practical realization of each of these approaches is always a compromise between numerical accuracy in the calculation of binding energies and the number of the nuclei included into the fitting protocol. This limitation is due to the restrictions in the availability of computational power. In such a situation, an ABOA emerges as a reasonable alternative to FGA and RGA. It provides a solution which is close to that obtained in RGA but at small portion of computational time required for RGA. The correction function of Eq. (2) provides a significant push to a minimum within one to three iterations of ABOA and the use of a softer correction function of Eq. (20) guaranties the smoothness of the convergence process at further iterations.
- Our analysis indicates that ten spherical anchor nuclei with experimental information on charge radii are sufficient for constraining the properties of charge radii globally in ABOA. Because of their single and doubly magic nature they are characterized by reduced theoretical uncertainties as compared with a global set of the data theoretical description of which will bring larger theoretical uncertainties. However, spin-orbit contributions to charge radii and the $\frac{N}{Z}r_n^2$ term of Eq. (25) have to be taken into account in the fit of the next generation of CEDFs. Note that unresolved *proton radius puzzle* puts a limit on the accuracy of the description of charge radii.
- For the first time, the numerical errors in binding energies related to the truncation of bosonic

¹³ This implies that for a best description of binding energies their calculations with the functionals created in such a way should be performed in the N_F basis used in the fitting protocol. Note that such philosophy also applies for non-relativistic functionals fitted in restricted basis without infinite basis corrections (such as UNEDF class of the Skyrme functionals) (see Ref. [69]).

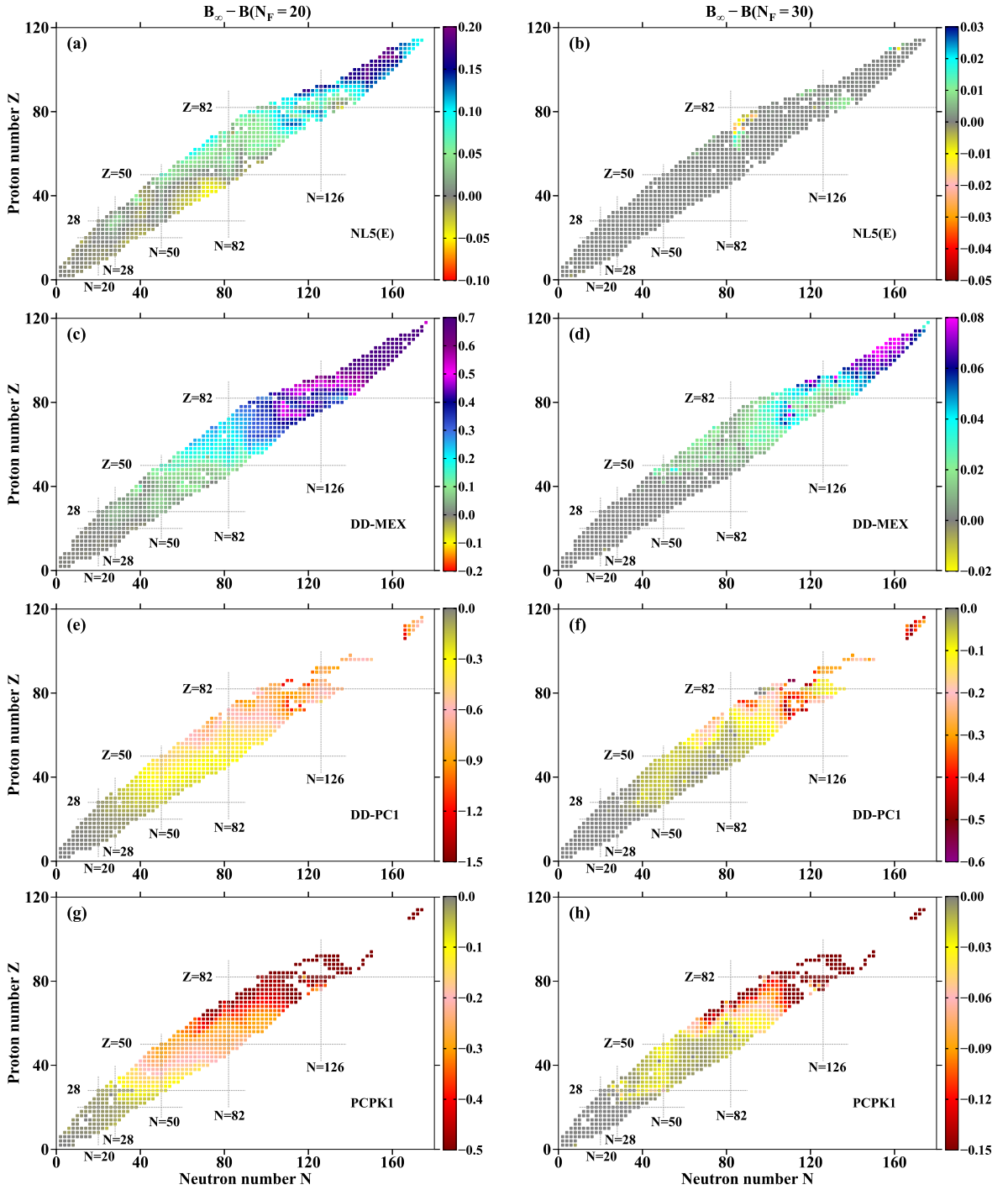


FIG. 10. The comparison of asymptotic binding energies with those obtained in the calculations with $N_F = 20$ and $N_F = 30$. White squares are used for the nuclei in which either the calculations with indicated truncations of the basis bring the quadrupole deformations β_2 which differ by more than 0.01 or the definition of B_∞ is not numerically possible. Note that the colormaps are different in different panels.

basis have been investigated in spherical and deformed nuclei with respect of asymptotic values corresponding to the infinite basis. It was shown that these errors increase with increasing the mass of the nucleus. They also increase on transition from

spherical to deformed nuclei. The dependence of these errors on the functional is weak. The truncation of bosonic basis at $N_B = 20$ provides a numerical error which is better than 50 keV in all nuclei with exception of superheavy ones with $Z \approx 120$

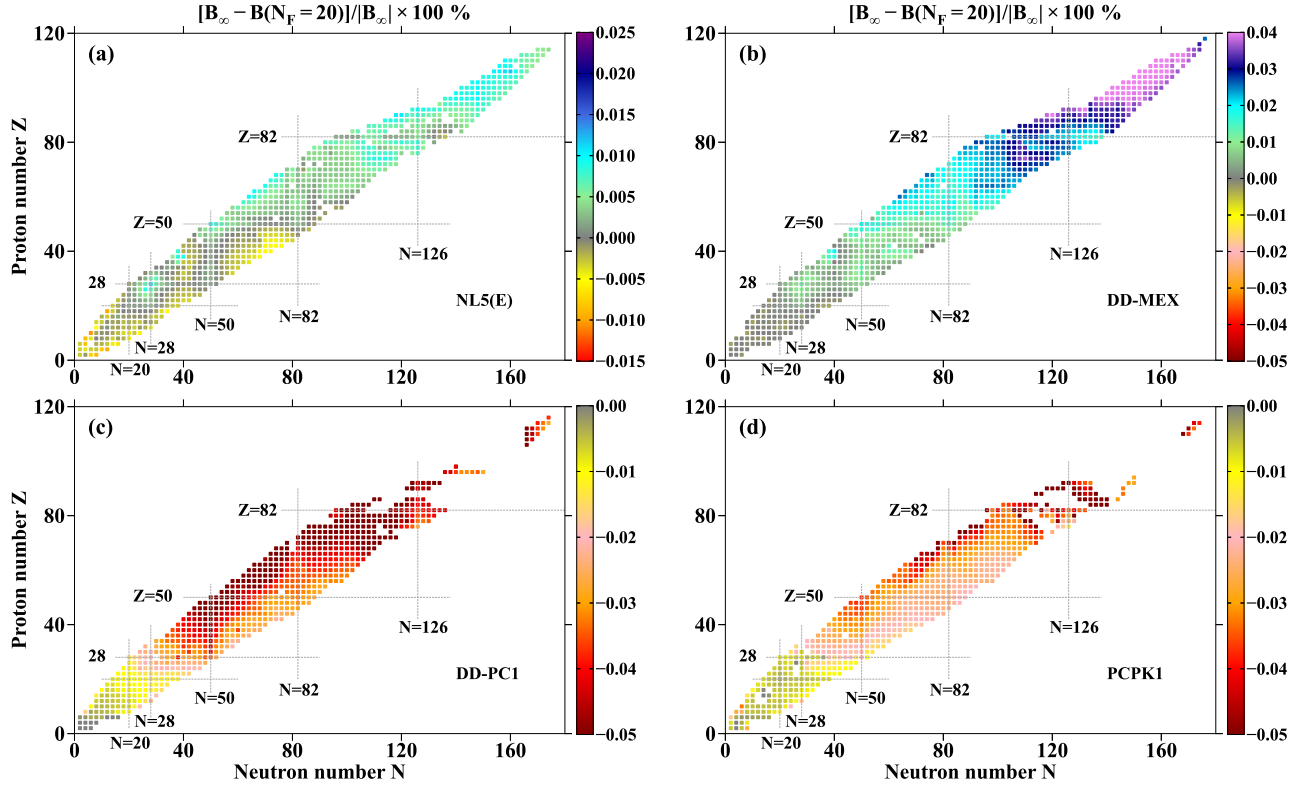


FIG. 11. Relative errors (in %) in the calculations of binding energies $B(N_F = 20)$ in the truncation of basis with $N_F = 20$ as compared with those (B_∞) obtained in the infinite basis. Note that the colormaps have different ranges: only in the case of the DD-PC1 and PC-PK1 functionals the same ranges are used. White squares are used for the nuclei in which either the calculations with the $N_F = 20$ and $N_F = 30$ bases bring the quadrupole deformations β_2 which differ by more than 0.01 or the definition of B_∞ is not numerically possible.

and $N \approx 184$. The increase of bosonic basis to $N_B = 28$, which is easily achievable at modern computers, will reduce this error to below 10 keV for almost all nuclei of interest.

- The numerical errors in binding energies related to the truncation of the fermionic basis have been systematically and globally investigated for the first time. A number of new results has been obtained. First, the way on how the calculated binding energies approach as a function of N_F their asymptotic values depends on the type of the functional. For example, for $N_F \geq 18$, the absolute values of binding energy increase with increasing N_F for the functionals which contain point coupling (PC-PK1 and DD-PC1) while it decreases for CEDFs which contain meson exchange (NL5(E), DD-ME2 and DD-MEX). Second, the convergence as a function of N_F depends on the class of CEDF: in a given nucleus, the fastest (at lower N_F) approach of asymptotic values of binding energies is seen in the NLME functionals, followed by the DDME ones and the PC functionals are characterized by the slowest convergence. Third, for a given functional, the increase of either mass or the deformation of nucleus requires the increase of the size of fermionic basis for ob-

taining asymptotic value of binding energy.

- The present paper clearly indicates the need for accounting of infinite basis corrections both for calculating the binding energies and their comparison with experimental data and for fitting of next generation of CEDFs. The current generation of CEDFs ignores these corrections. Although partially these corrections are built into the parameters of the functionals, this leads to some uncontrollable deviations in binding energies as compared with those obtained in the infinite basis. The existing prescription for finding asymptotic values of binding energy in the modest size basis which is used in non-relativistic DFTs does not provide high numerical accuracy and predictive power in the case of CDFT. An alternative procedure for finding the asymptotic values of binding energies has been suggested for the first time in the present paper (see Sec. VI). It is free from above mentioned deficiencies of non-relativistic prescription and allows better control of numerical errors in the definition of asymptotic binding energies.

The present paper clearly indicates that the binding energies of the nuclei represent the most numerically de-

manding type of physical observable among the ones considered at the mean field level. This is due to both their slow convergence as a function of N_F , the request for extremely high precision in their calculation in different subfields of nuclear physics and nuclear astrophysics as well as high precision of their experimental measurements. In contrast, accurate description of other physical observables (such as deformations, moments of inertia, etc) requires substantially smaller size of fermionic basis. The present paper also indicates the need for a new generation of CEDFs which takes into account infinite basis corrections in the calculation of binding energies. The work in defining such functionals is in progress and the results of such study will be reported later.

Note that the functionals studied in the present paper are restricted to the ones defined at the mean field level. However, the results obtained here can be generalized to the approaches which include correlations beyond mean field. For example, for that the RHB approach in the anchor based optimization method has to be replaced by an appropriate beyond-mean-field method (such as a five-dimensional collective Hamiltonian [70–72]). This will allow to bypass the existing challenge of extreme computational cost of fitting EDFs at the beyond-mean-field level and generate such functionals. It is expected that similar to non-relativistic (see, for example, Ref. [18]) and relativistic (see Refs. [63, 65]) DFT approaches this will lead to a further improvement of the description of binding energies. An alternative approach to the improvement of the description of binding energy is Bayesian Neural

Network (BNN) approach in which the fluctuating part of binding energy is described with the help of statistical methods (see, for example, Refs. [73, 74]). The BNN approaches improve the accuracy of the prediction of the binding energy at relatively modest numerical cost, provide statistical errors for predicted binding energies but do not generate a microscopic insight on the origin of the fluctuating part of binding energy which they improve.

Significant numerical cost associated with the solution of the Dirac equation in the CDFT framework calls for a search of alternative approaches to its solution. The use of Dirac oscillator basis (see Refs. [75, 76]) could be one of these alternatives. This, however, requires the development of the RHB code in the Dirac oscillator basis for axially deformed nuclei. It would be also interesting to investigate whether the reduced basis method for building of efficient and accurate emulators [77, 78] can be useful in the reduction of the computational cost. However, so far this method has been applied only to the single-particle energies and wavefunctions in spherical nuclei. Thus, the extension of this method to axially deformed nuclei and the investigations of both its accuracy in the calculation of binding energies and computational gains as compared with the method applied in the present paper are needed to establish its feasibility.

VIII. ACKNOWLEDGMENTS

This material is based upon work supported by the U.S. Department of Energy, Office of Science, Office of Nuclear Physics under Award No. DE-SC0013037.

-
- [1] W. Mittig, A. Lépine-Szily, and N. A. Orr, *Annu. Rev. Nucl. Sci.* **47**, 27 (2003).
 - [2] J. Dilling, K. Blaum, M. Brodeur, and S. Eliseev, *Annu. Rev. Nucl. Sci.* **68**, 45 (2018).
 - [3] J. Erler, N. Birge, M. Kortelainen, W. Nazarewicz, E. Olsen, A. M. Perhac, and M. Stoitsov, *Nature* **486**, 509 (2012).
 - [4] A. V. Afanasjev, S. E. Agbemava, D. Ray, and P. Ring, *Phys. Lett. B* **726**, 680 (2013).
 - [5] S. E. Agbemava, A. V. Afanasjev, D. Ray, and P. Ring, *Phys. Rev. C* **89**, 054320 (2014).
 - [6] M. Arnould, S. Goriely, and K. Takahashi, *Phys. Rep.* **450**, 97 (2007).
 - [7] J. J. Cowan, C. Sneden, J. E. Lawler, A. Aprahamian, M. Wiescher, K. Langanke, G. Martínez-Pinedo, and F.-K. Thielemann, *Rev. Mod. Phys.* **93**, 015002 (2021).
 - [8] N. Chamel and P. Haensel, *Living Rev. Relativity* **11**, 10 (2008).
 - [9] R. Lau, M. Beard, S. S. Gupta, A. V. Afanasjev, E. F. Brown, A. Deibel, L. R. Gasques, G. W. Hitt, W. R. Hix, L. Keek, P. Möller, A. S. P. S. Shternin, M. Wiescher, and Y. Xu, *The Astrophysical J.* **859**, 62 (2018).
 - [10] F. Tondeur, S. Goriely, J. M. Pearson, and M. Onsi, *Phys. Rev. C* **62**, 024308 (2000).
 - [11] M. Samyn, S. Goriely, P.-H. Heenen, J. M. Pearson, and F. Tondeur, *Nucl. Phys. A* **700**, 142 (2002).
 - [12] S. Goriely, N. Chamel, and J. M. Pearson, *Phys. Rev. C* **88**, 061302 (2013).
 - [13] M. Baldo, L. M. Robledo, P. Schuck, and X. Viñas, *Phys. Rev. C* **87**, 064305 (2013).
 - [14] P. Möller, A. J. Sierk, T. Ichikawa, and H. Sagawa, *At. Data and Nucl. Data Tables* **109**, 1 (2016).
 - [15] M. Kortelainen, T. Lesinski, J. Moré, W. Nazarewicz, J. Sarich, N. Schunck, M. V. Stoitsov, and S. Wild, *Phys. Rev. C* **82**, 024313 (2010).
 - [16] M. Kortelainen, J. McDonnell, W. Nazarewicz, P.-G. Reinhard, J. Sarich, N. Schunck, M. V. Stoitsov, and S. M. Wild, *Phys. Rev. C* **85**, 024304 (2012).
 - [17] M. Kortelainen, J. McDonnell, W. Nazarewicz, E. Olsen, P.-G. Reinhard, J. Sarich, N. Schunck, S. M. Wild, D. Davesne, J. Erler, and A. Pastore, *Phys. Rev. C* **89**, 054314 (2014).
 - [18] S. Goriely, S. Hilaire, M. Girod, and S. Péru, *Phys. Rev. Lett.* **102**, 242501 (2009).
 - [19] D. Peña-Arteaga, S. Goriely, and N. Chamel, *Eur. Phys. J. A* **52**, 320 (2016).
 - [20] A. Taninah and A. V. Afanasjev, *Phys. Rev. C* **107**, L041301 (2023).
 - [21] P.-G. Reinhard, M. Rufa, J. Maruhn, W. Greiner, and J. Friedrich, *Z. Phys. A* **323**, 13 (1986).
 - [22] D. Vretenar, A. V. Afanasjev, G. A. Lalazissis, and P. Ring, *Phys. Rep.* **409**, 101 (2005).

- [23] B. Wei, Q. Zhao, Z.-H. Wang, J. Geng, B.-Y. Sun, Y.-F. Niu, and W.-H. Long, *Chinese Physics C* **44**, 074107 (2020).
- [24] J. Dobaczewski, M. V. Stoitsov, and W. Nazarewicz, *AIP Conf. Proc.* **726**, 51 (2004).
- [25] J. C. Pei, M. V. Stoitsov, G. I. Fann, W. Nazarewicz, N. Schunck, and F. R. Xu, private communication **78**, 064306 (2008).
- [26] C. Gonzalez-Boquera, M. Centelles, X. Vinas, and L. M. Robledo, *Phys. Lett. B* **779**, 195 (2018).
- [27] S. Goriely, private communication (2023).
- [28] S. Goriely, N. Chamel, and J. M. Pearson, *Phys. Rev. C* **93**, 034337 (2016).
- [29] S. Goriely, private communication (2023).
- [30] P. W. Zhao, Z. P. Li, J. M. Yao, and J. Meng, *Phys. Rev. C* **82**, 054319 (2010).
- [31] A. Taninah, S. E. Agbemava, A. V. Afanasjev, and P. Ring, *Phys. Lett. B* **800**, 135065 (2020).
- [32] T. Nikšić, D. Vretenar, and P. Ring, *Phys. Rev. C* **78**, 034318 (2008).
- [33] T. Nikšić, N. Paar, D. Vretenar, and P. Ring, *Comp. Phys. Comm.* **185**, 1808 (2014).
- [34] Y. K. Gambhir, P. Ring, and A. Thimet, *Ann. Phys. (N.Y.)* **198**, 132 (1990).
- [35] J. Boguta and R. Bodmer, *Nucl. Phys.* **A292**, 413 (1977).
- [36] S. Typel and H. H. Wolter, *Nucl. Phys.* **A656**, 331 (1999).
- [37] T. Bürvenich, D. G. Madland, J. A. Maruhn, and P.-G. Reinhard, *Phys. Rev. C* **65**, 044308 (2002).
- [38] G. A. Lalazissis, T. Nikšić, D. Vretenar, and P. Ring, *Phys. Rev. C* **71**, 024312 (2005).
- [39] X. Roca-Maza, X. Viñas, M. Centelles, P. Ring, and P. Schuck, *Phys. Rev. C* **84**, 054309 (2011).
- [40] S. E. Agbemava, A. V. Afanasjev, and A. Taninah, *Phys. Rev. C* **99**, 014318 (2019).
- [41] M. Wang, G. Audi, F. G. Kondev, W. Huang, S. Naimi, and X. Xu, *Chinese Physics C* **41**, 030003 (2017).
- [42] W. H. Press, S. A. Teukolsky, W. T. Vetterling, and B. P. Flannery, *Numerical recipes in Fortran 77. The art of scientific computing*. (2d Edition, Cambridge University Press, Cambridge, 2007).
- [43] I. Angeli and K. P. Marinova, *At. Data Nucl. Data Tables* **99**, 69 (2013).
- [44] M. Dutra, O. Lourenco, S. S. Avancini, B. V. Carlson, A. Delfino, D. P. Menezes, C. Providencia, S. Typel, and J. R. Stone, *Phys. Rev. C* **90**, 055203 (2014).
- [45] C. J. Horowitz and J. Piekarewicz, *Phys. Rev. C* **86**, 045503 (2012).
- [46] H. Kurasawa and T. Suzuki, *Prog. Th. Exp. Phys.* **2019**, 113D01 (2019).
- [47] J. L. Friar and J. W. Negele, *Adv. Nucl. Phys* **8**, 219 (1975).
- [48] P.-G. Reinhard and W. Nazarewicz, *Phys. Rev. C* **103**, 054310 (2021).
- [49] T. Naito, G. Colò, H. Liang, and X. Roca-Maza, *Phys. Rev. C* **104**, 024316 (2021).
- [50] P. A. Zyla, R. M. Barnett, J. Beringer, O. Dahl, D. A. Dwyer, D. E. Groom, C.-J. Lin, K. S. Lugovsky, E. Pianori, D. J. Robinson, C. G. Wohl, W.-M. Yao, K. Agashe, G. Aielli, B. C. Allanach, C. Am- sler, M. Antonelli, E. C. Aschenauer, D. M. Asner, H. Baer, S. Banerjee, L. Baudis, C. W. Bauer, J. J. Beatty, V. I. Belousov, S. Bethke, A. Bettini, O. Biebel, K. M. Black, E. Blucher, O. Buchmuller, V. Burkert, M. A. Bychkov, R. N. Cahn, M. Carena, A. Ceccucci, A. Cerri, D. Chakraborty, R. S. Chivukula, G. Cowan, G. D'Ambrosio, T. Damour, D. de Florian, A. de Gouvêa, T. DeGrand, P. de Jong, G. Dissertori, B. A. Dobrescu, M. D'Onofrio, M. Doser, M. Drees, H. K. Dreiner, P. Eerola, U. Egede, S. Eidelman, J. Ellis, J. Erler, V. V. Ezhela, W. Fetscher, B. D. Fields, B. Foster, A. Freitas, H. Gallagher, L. Garren, H.-J. Gerber, G. Gerbier, T. G. and Y. Gershtein, T. Gherghetta, A. A. Godizov, M. C. Gonzalez-Garcia, M. Goodman, C. Grab, A. V. Gritsan, C. Grojean, M. Grünewald, A. Gurtu, T. Gutsche, H. E. Haber, C. Hanhart, S. Hashimoto, Y. Hayato, A. Hebecker, S. Heinemeyer, B. Heltsley, J. J. Hernández-Rey, K. Hikasa, J. Hisano, A. Höcker, J. Holder, A. Holtkamp, J. Huston, T. Hyodo, K. F. Johnson, M. Kado, M. Karliner, U. F. Katz, M. Kenzie, V. A. Khoze, S. R. Klein, E. Klempt, R. V. Kowalewski, F. Krauss, M. Kreps, B. Krusche, Y. Kwon, O. Lahav, J. Laiho, L. P. Lellouch, J. Lesgourgues, A. R. Liddle, Z. Ligeti, C. Lippmann, T. M. Liss, L. Littenberg, C. Lourenco, S. B. Lugovsky, A. Lusiani, Y. Makida, F. Maltoni, T. Mannel, A. V. Manohar, W. J. Marciano, A. Masoni, J. Matthews, U.-G. Meißner, M. Mikhasenko, D. J. Miller, D. Milstead, R. E. Mitchell, K. Mönig, P. Molaro, F. Moortgat, M. Moskvic, K. Nakamura, M. Narain, P. Nason, S. Navas, M. Neubert, P. Nevski, Y. Nir, K. A. Olive, C. Patrignani, J. A. Peacock, S. T. Petcov, V. A. Petrov, A. Pich, A. Piepke, A. Pomarol, S. Profumo, A. Quadt, K. Rabbertz, J. Rademacker, G. Raffelt, H. Ramani, M. Ramsey-Musolf, B. N. Ratcliff, P. Richardson, A. Ringwald, S. Roesler, S. Rolli, A. Romaniouk, L. J. Rosenberg, J. L. Rosner, G. Rybka, M. Ryskin, R. A. Ryutin, Y. Sakai, G. P. Salam, S. Sarkar, F. Sauli, O. Schneider, K. Scholberg, A. J. Schwartz, J. Schwiening, D. Scott, V. Sharma, S. R. Sharpe, T. Shutt, M. Silari, T. Sjöstrand, P. Skands, T. Skwarnicki, G. F. Smoot, A. Soffer, M. S. S. S. Spanier, C. Spiering, A. Stahl, S. L. Stone, Y. Sumino, T. Sumiyoshi, M. J. Syphers, F. Takahashi, M. Tanabashi, J. Tanaka, M. Taševský, K. Terashi, J. Terning, U. Thoma, R. S. Thorne, L. Tiator, M. Titov, N. P. Tkachenko, D. R. Tovey, K. Trabelsi, P. Urquijo, G. Valencia, R. V. de Water, N. Varelas, G. Venanzoni, L. Verde, M. G. Vinciter, P. Vogel, W. Vogelsang, A. Vogt, V. Vorobyev, S. P. Wakely, W. Walkowiak, C. W. Walter, D. Wands, M. O. Wascko, D. H. Weinberg, E. J. Weinberg, M. White, L. R. Wiencke, S. Willocq, C. L. Woody, R. L. Workman, M. Yokoyama, R. Yoshida, G. Zanderighi, G. P. Zeller, O. V. Zenin, R.-Y. Zhu, and S.-L. Zhu, *Prog. Theor. Part. Phys.* **083C01** (2020).
- [51] I. Sick, *Atoms* **6**, 1 (2018).
- [52] H. Gao and M. Vanderhaeghen, *Rev. Mod. Phys.* **94**, 015002 (2022).
- [53] U. C. Perera, A. V. Afanasjev, and P. Ring, *Phys. Rev. C* **104**, 064313 (2021).
- [54] P. Campbell, I. Moore, and M. Pearson, *Prog. Part. Nucl. Phys.* **86**, 127 (2016).
- [55] T. Naito, T. Oishi, H. Sagawa, and Z. Wang, *Phys. Rev. C* **107**, 054307 (2022).
- [56] U. C. Perera and A. V. Afanasjev, *Phys. Rev. C* **107**, 064321 (2023).
- [57] L. Bonneau, P. Quentin, and P. Möller, *Phys. Rev. C* **76**, 024320 (2007).

- [58] E. V. Litvinova and A. V. Afanasjev, *Phys. Rev. C* **84**, 014305 (2011).
- [59] J. Dobaczewski, A. V. Afanasjev, M. Bender, L. M. Robledo, and Y. Shi, *Nucl. Phys. A* **944**, 388 (2015).
- [60] G. A. Lalazissis, S. Raman, and P. Ring, *At. Data Nucl. Data Table* **71**, 1 (1999).
- [61] L. Geng, H. Toki, and J. Meng, *Prog. Theor. Phys.* **113**, 785 (2005).
- [62] P.-G. Reinhard and B. K. Agrawal, *Int. Jour. Mod. Phys. E* **20**, 1379 (2011).
- [63] Q. S. Zhang, Z. M. Niu, Z. P. Li, J. M. Yao, and J. Meng, *Frontiers of Physics* **9**, 529 (2014).
- [64] K. Q. Lu, Z. X. Li, Z. P. Li, J. M. Yao, and J. Meng, *Phys. Rev. C* **91**, 027304 (2015).
- [65] Y. L. Yang, Y. K. Wang, P. W. Zhao, and Z. P. Li, *Phys. Rev. C* **104**, 054312 (2021).
- [66] S. E. Agbemava, A. V. Afanasjev, A. Taninah, and A. Gyawali, *Phys. Rev. C* **99**, 034316 (2019).
- [67] P.-G. Reinhard, *Rep. Prog. Phys.* **52**, 439 (1989).
- [68] S. Hilaire and M. Girod, *Eur. Phys. J.* **33**, 237 (2007).
- [69] M. Kortelainen, private communication (2023).
- [70] T. Nikšić, Z. P. Li, D. Vretenar, L. Próchniak, J. Meng, and P. Ring, *Phys. Rev. C* **79**, 034303 (2009).
- [71] Z. P. Li, T. Nikšić, D. Vretenar, J. Meng, G. A. Lalazissis, and P. Ring, *Phys. Rev. C* **79**, 054301 (2009).
- [72] Z. Shi, A. V. Afanasjev, Z. P. Li, and J. Meng, *Phys. Rev. C* **99**, 064316 (2019).
- [73] R. Utama, J. Piekarewicz, and H. B. Prosper, *Phys. Rev. C* **93**, 014311 (2016).
- [74] L. Neufcourt, Y. Cao, W. Nazarewicz, and F. Viens, *Phys. Rev. C* **98**, 034318 (2018).
- [75] M. Moshinsky and A. Szczepaniak, *Journal of Physics A: Mathematical and General* **22**, L817 (1989).
- [76] J. Yang and J. Piekarewicz, *Phys. Rev. C* **102**, 054308 (2020).
- [77] E. Bonilla, P. Giuliani, K. Godbey, and D. Lee, *Phys. Rev. C* **106**, 054322 (2022).
- [78] A. L. Anderson, G. L. O'Donnell, and J. Piekarewicz, *Phys. Rev. C* **106**, L031302 (2022).